



Variationally consistent homogenization of diffusion in particle composites with material interfaces using dual macroscale chemical potentials

Downloaded from: <https://research.chalmers.se>, 2025-04-01 10:28 UTC

Citation for the original published paper (version of record):

Rollin, D., Larsson, F., Runesson, K. et al (2025). Variationally consistent homogenization of diffusion in particle composites with material interfaces using dual macroscale chemical potentials. *Computational Mechanics*, In Press. <http://dx.doi.org/10.1007/s00466-025-02605-5>

N.B. When citing this work, cite the original published paper.



Variationally consistent homogenization of diffusion in particle composites with material interfaces using dual macroscale chemical potentials

David René Rollin¹ · Fredrik Larsson² · Kenneth Runesson² · Ralf Jänicke¹

Received: 22 July 2024 / Accepted: 27 January 2025
© The Author(s) 2025

Abstract

Computational homogenization of particle-matrix composites with material interfaces is considered, whereby linear transient diffusion driven by a chemical potential is used as a model problem. Due to the models linearity, it is beneficial to assume micro-stationarity in order to provide direct upscaling and avoid excessive computational cost. First order homogenization with a single macroscale chemical potential is taken as the most basic approach; however, the accuracy is negatively affected whenever relevant micro-transient effects can not be captured using the stationary sub-scale problem. To improve the accuracy while still upscaling from a stationary sub-scale problem, different formulations based on dual macroscale potentials, one for each phase, are proposed and investigated in this paper. As to the prolongation order within the particles and matrix phase, respectively, two types are considered: constant-linear and linear-linear. Most importantly, for the case of linear prolongation, different ways of defining the macroscale variables (acting as loading on the RVE-problem) in terms of suitable measures of the chemical potential can be envisioned: (1) averaging of 0th and 1st gradient of the potential, (2) averaging of 0th and 1st moment of the potential. The pros and cons of the different approaches were assessed in a numerical study and compared to a reference solution from Direct Numerical Simulation (DNS) for an example problem. It was concluded that the moment-based linear-linear method was the only one that could match the DNS solution for all considered material parameters. However, for sufficiently large interface resistance, leading to a more pronounced potential jump across the interfaces, the constant-linear prolongation gave comparable results.

Keywords Variationally consistent homogenization · Diffusion · Multi-scale modeling · Particle-matrix composites · Interfaces

1 Introduction

Composite materials often comprise two, or more, distinct phases that have different constitutive character depending

on the sub-scale structure. A large subclass of composites is characterized by particles that are embedded in a contiguous matrix, whereby the particles are not in contact with each other. Regarding diffusive processes in such a composite, its effective properties depend on the characteristics of the underlying phases as well as the transport across the interfaces.

The interface between particles and matrix is associated with surface-specific material properties. For diffusive transport at an interface, the most general imperfect interface is characterized by a discontinuity in the primary field as well as the normal component of the flux, cf. [1–5], whereby constitutive relations are required for the flux in terms of the primary field on each side of the interface. A simplified situation is at hand when the flux is continuous and depends only on the jump of the primary field, cf. cohesive zone modeling of ductile fracture (whereby the traction is assumed

✉ David René Rollin
d.rollin@tu-braunschweig.de

Fredrik Larsson
fredrik.larsson@chalmers.se

Kenneth Runesson
kenneth.runesson@chalmers.se

Ralf Jänicke
r.janicke@tu-braunschweig.de

¹ Institute of Applied Mechanics, Technische Universität Braunschweig, 38106 Braunschweig, Germany

² Department of Industrial and Materials Science, Chalmers University of Technology, SE-41296 Gothenburg, Sweden

to depend on the displacement jump across the interface). It is, indeed, possible to use the analogous argument for other (multi)physics problems incorporating (inter)actions of mechanical, electrical and thermal nature. Prominent examples of multi-functional composites involving multi-physics interactions are: active electrode materials in batteries, electric conductors, piezo-electric actuators and sensors, and concrete structures, to name a few.

Computational homogenization has been exploited extensively in the past, either as a method to compute effective properties or as part of an FE²-strategy, to analyze composites with various micro-heterogeneous complexity [5–13]. In this paper, we investigate a model problem of linear diffusion in a particle-matrix composite, whereby the primary field in a straightforward weak setting (on the fine-scale) is the chemical potential. Methods exist for assumed perfect interfaces [14–19], however, we consider the possibility for a potential jump at the interface, while assuming a continuous flux across the interface.

In terms of Variationally Consistent Homogenization (VCH), cf. [16, 20–23], the corresponding straightforward approach is to introduce a linear prolongation of a *single macroscale potential* that represents the composite behavior. This type of approach has been employed for materials like poly-crystals [10, 11], but it can have shortcomings when applied to particle-matrix composites. In case of a large contrast in mobilities of the materials or a high interface resistance, the micro-transient effect could only be captured by upscaling from a transient Representative Volume Element (RVE) problem. For a linear problem, this implies that direct upscaling is no longer possible, which would be computationally less expensive.

Clearly, it is possible to compute the true fluctuation including discontinuity across the interfaces only via Direct Numerical Simulation (DNS), although such an approach is hardly computationally feasible in practice. However, in those cases when the phase mobilities are greatly different, or the interface resistance is high, we can expect that the fine-scale solution of the chemical potential shows significant heterogeneity [15, 24]. Consequently, it is conjectured that it is necessary to improve the accuracy of the numerical algorithm by introducing dual macroscale chemical potentials [15]. Whereas each potential coexist on the macroscale, they represent the prolongation only within its respective phase domain (particle and matrix) in the RVE. Such an approach is discussed in [25] using asymptotic expansion for the limit of perfect separation of scales.

This paper is outlined as follows: In Sect. 2, the balance and constitutive equations on the fine-scale are introduced. In Sect. 3, we introduce the VCH procedure in the context of first order homogenization (linear prolongation) with a single macroscale potential. The different approaches to defining the macroscale variables are outlined. Further, the short-

comings of the single potential approach are discussed as a motivation for the subsequent proposals. Next, in Sect. 4, two alternative choices of prolongation are presented in the context of VCH with dual macroscale chemical potentials: *constant-linear* and *linear-linear*. In Sect. 5, an upscaling procedure is presented: Under the assumption of micro-stationarity, sensitivities are used to exploit the linearity of the model. In Sect. 6, an example problem is analyzed with the purpose to compare the results of the different approaches to a reference solution from DNS. Finally, concluding remarks and an outlook to future work are given in Sect. 7.

Regarding notation, meager type is used to denote scalars, whereas bold type is used to denote vectors as well as higher order tensors. Scalar product (single contraction) is denoted by a dot. For example, for two vectors \mathbf{a} , \mathbf{b} and a second order tensor \mathbf{A} , we have $\mathbf{a} \cdot \mathbf{b} = a_i b_i$ and $(\mathbf{A} \cdot \mathbf{b})_i = (\mathbf{A})_{ij} (\mathbf{b})_j$ in terms of their Cartesian components, where the Einstein summation convention is used. To be consistent with index notation, $\diamond \cdot \nabla$ (and not $\nabla \cdot \diamond$) denotes the divergence (i.e. $(\diamond)_{ij,j}$).

Homogenization is carried out on given realization of the microstructure, defined by an RVE; however, whether the RVE is actually representative is not an issue in this paper. The phases of particles, matrix as well as their interface are referred to using the indices p, m and i, respectively. Volume, interface and surface averages of an intensive field \diamond are denoted

$$\langle \diamond \rangle_{\square}^p := \frac{1}{|\Omega_{\square}^p|} \int_{\Omega_{\square}^p} \diamond d\Omega, \quad (1a)$$

$$\langle \diamond \rangle_{\square}^m := \frac{1}{|\Omega_{\square}^m|} \int_{\Omega_{\square}^m} \diamond d\Omega, \quad (1b)$$

$$\langle \diamond \rangle_{\square} := \langle \diamond \rangle_{\square}^p + \langle \diamond \rangle_{\square}^m, \quad (1c)$$

$$\langle \diamond \rangle^p := \frac{1}{|\Omega_{\square}^p|} \int_{\Omega_{\square}^p} \diamond d\Omega, \quad (1d)$$

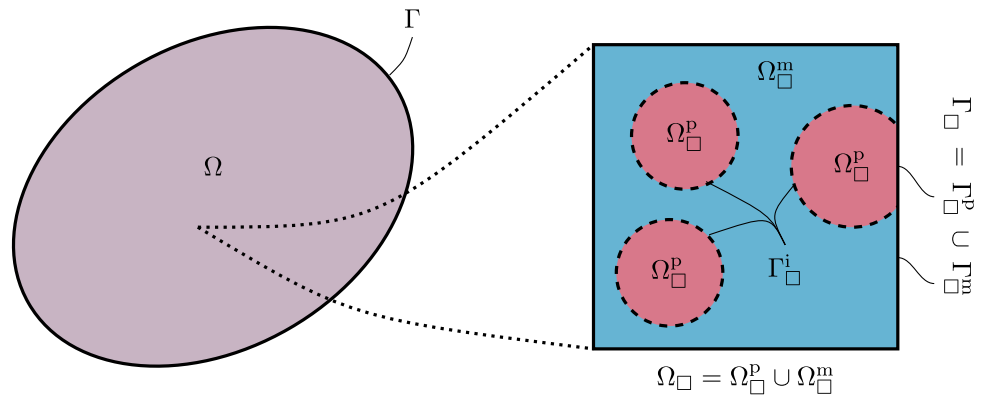
$$\langle \diamond \rangle^m := \frac{1}{|\Omega_{\square}^m|} \int_{\Omega_{\square}^m} \diamond d\Omega, \quad (1e)$$

$$\langle \langle \diamond \rangle \rangle_{\square}^i := \frac{1}{|\Omega_{\square}|} \int_{\Gamma_{\square}^i} \diamond d\Gamma, \quad (1f)$$

$$\langle \langle \diamond \rangle \rangle_{\square} := \frac{1}{|\Omega_{\square}|} \int_{\Gamma_{\square}} \diamond d\Gamma, \quad (1g)$$

where Ω_{\square} is the RVE domain, Γ_{\square} is its boundary, $(\Omega_{\square}^p, \Omega_{\square}^m, \Gamma_{\square}^p, \Gamma_{\square}^m)$ are associated with the corresponding phases, and Γ_{\square}^i is the interface between particles and matrix. A sketch of an RVE with these definitions is given in Fig. 1. For a quantity \diamond which exhibits a jump at the interface, its value on the particle side is denoted \diamond^p and on the matrix side \diamond^m , respectively. The macroscale representation of a quantity \diamond is denoted $\bar{\diamond}$. Further, the operator $\partial_t \diamond$ is used for the derivative with respect to time.

Fig. 1 Sketch of the computational domain and an RVE of a particle-matrix composite



2 Fine-scale model

The model problem of linear transient diffusion is defined in what follows: Consider a domain Ω comprising particles Ω^p that are embedded in a matrix Ω^m with interfaces Γ^i . We introduce a chemical potential $\mu(\mathbf{x}, t) : \Omega^p \cup \Omega^m \times \mathbb{R}^+ \rightarrow \mathbb{R}$ as the primary field. We also define the molar concentration c of the diffusing species and the molar flux density \mathbf{j} , cf. [20, 26]. Within the two phase domains, we define the chemical potential gradient $\zeta[\mu] := \nabla\mu$.

The mass balance in the bulk materials and the interface condition are stated as

$$\partial_t c + \mathbf{j} \cdot \nabla = 0 \quad \text{in } (\Omega^p \cup \Omega^m) \times (0, T], \quad (2a)$$

$$j_n^p + j_n^m = 0 \quad \text{on } \Gamma^i \times (0, T], \quad (2b)$$

where we introduced the normal flux quantities $j_n^p := \mathbf{j}^p \cdot \mathbf{n}^p$ and $j_n^m := \mathbf{j}^m \cdot \mathbf{n}^m$, and where $(\mathbf{n}^p, \mathbf{n}^m)$ are the normal vectors pointing out of the corresponding domains. Note that only the normal flux (component) across the interface is accounted for. In general, tangential fluxes associated with transport parallel to the interface can occur, cf. [1]. This would imply storage of the species inside the interface and the possibility of jumps in the normal flux on both sides of the interface, which is not considered here.

The initial state is defined by $c(\mathbf{x}, t = 0) = c_0(\mathbf{x})$. Boundary conditions on $\Gamma = \partial\Omega = \Gamma_D \cup \Gamma_N$ in terms of prescribed potential μ^{pre} and normal flux density j_n^{pre} are defined as

$$\mu = \mu^{\text{pre}} \quad \text{on } \Gamma_D \times (0, T], \quad (3a)$$

$$\mathbf{j} \cdot \mathbf{n} = j_n^{\text{pre}} \quad \text{on } \Gamma_N \times (0, T]. \quad (3b)$$

Constitutive relations with isotropic bulk mobility η and interface mobility¹ η_{if} are chosen as

$$\mathbf{j}(\zeta) = -\eta\zeta, \quad (4a)$$

¹ The term mobility is not referring to a motion, but to the fact that the chemical potential drives the fluxes (not the concentration).

$$j_n(\llbracket\mu\rrbracket) := j_n^p = -\eta_{if}\llbracket\mu\rrbracket, \quad (4b)$$

$$c(\mu) = c_{\text{ref}} + \frac{c_m}{R\theta_{\text{ref}}}\llbracket\mu - \mu_{\text{ref}}\rrbracket, \quad (4c)$$

where $\llbracket\mu\rrbracket := \mu^m - \mu^p$ is the potential jump at the interface. Moreover, (4c) follows from a linearization of an expression of the form $\mu(c) = R\theta_{\text{ref}} \log(\frac{c}{\gamma(c)})$, where θ_{ref} is a reference temperature and R is the universal gas constant. The material parameter c_m is a result of the general linearization [21]. Note that the linearity of relation (4c) can be used to state the problem with c as primary variable without any disadvantages. However, for a more complex model of $\mu(c)$ and/or for multi-field problems, e.g. a chemo-mechanically coupled problem, it is advantageous to keep μ as the primary field [26].

Finally, using the notation $\delta\zeta := \zeta[\delta\mu]$, the weak form of the balance equations can be stated as follows: For given $\mu^{\text{pre}}(t)$, $j_n^{\text{pre}}(t)$, find $\mu(\bullet, t) \in \mathbb{M}$ that solves

$$\begin{aligned} & \int_{\Omega} \partial_t c \delta\mu - \mathbf{j} \cdot \delta\zeta \, d\Omega - \int_{\Gamma^i} j_n \llbracket\delta\mu\rrbracket \, d\Gamma \\ & = \int_{\Gamma_N} -j_n^{\text{pre}} \delta\mu \, d\Gamma \quad \forall \delta\mu \in \mathbb{M}^0, \end{aligned} \quad (5)$$

where \mathbb{M} and \mathbb{M}^0 are the appropriately defined solution and test function space, respectively.

3 Variationally consistent homogenization - single potential approach

3.1 Macroscale problem

As a first step in the VCH framework, running averages are introduced for the integrands in the weak form (5) of the fine-scale model, which gives

$$\int_{\Omega} \langle \partial_t c \delta\mu - \mathbf{j} \cdot \delta\zeta \rangle_{\square} - \langle \langle j_n \llbracket\delta\mu\rrbracket \rangle \rangle_{\square}^i \, d\Omega$$

$$= \int_{\Gamma_N} -j_n^{\text{pre}} \delta \mu \, d\Gamma \quad \forall \delta \mu \in \bar{\mathbb{M}}^0. \quad (6)$$

Next, the potential is additively decomposed into a smooth macroscale contribution μ^M and a fluctuating sub-scale part μ^s as

$$\mu = \mu^M + \mu^s. \quad (7)$$

In the single potential approach, the macroscale contribution μ^M within a given RVE domain is prolonged from a single macroscale potential $\bar{\mu} \in \bar{\mathbb{M}}$. In the case of first order homogenization, this relation can be defined by

$$\mu^M[\bar{\mu}](\bar{\mathbf{x}}, \mathbf{x}) = \bar{\mu}(\bar{\mathbf{x}}) + \bar{\boldsymbol{\zeta}}(\bar{\mathbf{x}}) \cdot [\mathbf{x} - \bar{\mathbf{x}}], \quad \mathbf{x} \in \Omega_{\square}^p \cup \Omega_{\square}^m, \quad (8)$$

where $\bar{\boldsymbol{\zeta}} := \nabla \bar{\mu}$. The two-scale problem can be derived by inserting (7) and (8) into (6): For given $\mu^{\text{pre}}(t)$, $j_n^{\text{pre}}(t)$, find $\bar{\mu}(\bullet, t) \in \bar{\mathbb{M}}$, $\mu^s(\bullet, t) \in \bar{\mathbb{M}}^s$ that solve

$$\begin{aligned} & \int_{\Omega} \langle \partial_t c [\mu^M[\delta \bar{\mu}] + \delta \mu^s] \rangle_{\square} \, d\Omega \\ & - \int_{\Omega} \langle \mathbf{j}(\boldsymbol{\zeta} [\mu^M[\bar{\mu}] + \mu^s]) \cdot \boldsymbol{\zeta} [\mu^M[\delta \bar{\mu}] + \delta \mu^s] \rangle_{\square} \, d\Omega \\ & - \int_{\Omega} \langle \langle j_n(\llbracket \mu^M[\bar{\mu}] + \mu^s \rrbracket) \rrbracket \mu^M[\delta \bar{\mu}] + \delta \mu^s \rangle \rangle_{\square}^i \, d\Omega \\ & = \int_{\Gamma_N} -j_n^{\text{pre}} [\mu^M[\delta \bar{\mu}] + \delta \mu^s] \, d\Gamma \\ & \forall (\delta \bar{\mu}, \delta \mu^s) \in \bar{\mathbb{M}}^0 \times \bar{\mathbb{M}}^{s,0}. \end{aligned} \quad (9)$$

The macroscale problem is derived from (9) by the choice $\delta \mu^s = 0$. We assume that j_n^{pre} is smooth enough such that boundary conditions can be expressed by prescribed values \bar{j}_n^{pre} and $\bar{\mu}^{\text{pre}}$. With the definition $\delta \bar{\boldsymbol{\zeta}} := \nabla \delta \bar{\mu}$, the macroscale problem reads: For given $\bar{\mu}^{\text{pre}}(t)$, $\bar{j}_n^{\text{pre}}(t)$, find $\bar{\mu}(\bullet, t) \in \bar{\mathbb{M}}$ that satisfies

$$\int_{\Omega} \partial_t \bar{c} \delta \bar{\mu} - (\bar{\mathbf{j}} - \partial_t \bar{\mathbf{c}}_2) \cdot \delta \bar{\boldsymbol{\zeta}} \, d\Omega = \int_{\Gamma_N^p} -\bar{j}_n^{\text{pre}} \delta \bar{\mu} \, d\Gamma \quad \forall \delta \bar{\mu} \in \bar{\mathbb{M}}^0, \quad (10)$$

where the (variationally consistent) homogenized fields are given as

$$\bar{c} := \langle c \rangle_{\square}, \quad \bar{\mathbf{c}}_2 := \langle c[\mathbf{x} - \bar{\mathbf{x}}] \rangle_{\square}, \quad \bar{\mathbf{j}} := \langle \mathbf{j} \rangle_{\square}, \quad (11)$$

and the solution and test function spaces are

$$\bar{\mathbb{M}} = \{\mu \in \mathbb{H}^1(\Omega) : \mu|_{\Gamma_D} = \bar{\mu}^{\text{pre}}\}, \quad (12a)$$

$$\bar{\mathbb{M}}^0 = \{\mu \in \mathbb{H}^1(\Omega) : \mu|_{\Gamma_D} = 0\}. \quad (12b)$$

Here, $\mathbb{H}^1(\bullet)$ denotes the Sobolev space of functions with square integrable 0th and 1st order derivatives.

It is noted that the macroscale problem has the same structure as the fine-scale problem, with an important exception: $\llbracket \mu^M \rrbracket$ vanishes, which means that the transport across the interface is not explicitly accounted for in the macroscale problem. In case of a high resistance at the interface, this introduces an inaccuracy, which can be seen in the numerical study in Sect. 6. Overcoming this drawback is one motivation for the dual potential approach which is presented in Sect. 4.

3.2 RVE-problem

3.2.1 Preliminaries

To derive an RVE-problem from (9), homogenization constraints and boundary conditions need to be defined. The homogenization constraints define how given macroscopic data ($\bar{\mu}$, $\bar{\boldsymbol{\zeta}}$) are accounted for in the solution of the RVE-problem. Most importantly, they ensure solvability of the RVE-problem and a unique hierarchical decomposition into macroscale and fluctuating parts, cf. [22]. Subsequently, two possible choices are presented. One is based on the average of the 0th and 1st gradient of the potential, whereas the other is based on the average of the 0th and 1st moment of the potential. The latter is motivated by the disjunct particle domains in combination with material interfaces. In this case, for the particle domain, local gradients are insufficient for a proper kinematical connection of fine-scale and macroscale fields. For example, given a fine-scale field, it would be possible to have non-zero macroscale gradients for adjacent RVEs with the same macroscale potential, cf. Figure 2. This problem arises for the dual potential approach, where matrix and particle domain are treated separately in the homogenization procedure. A demonstration of the problematic RVE response is given later in Sect. 6.2. We propose to use the average moment instead of the average gradient to overcome this issue.

3.2.2 RVE-problem for gradient-based constraints

The standard format of homogenization constraints is based on the 0th and 1st order gradients of the fine-scale potential μ and can be expressed as

$$\langle \mu \rangle_{\square} = \bar{\mu}, \quad \langle \boldsymbol{\zeta}[\mu] \rangle_{\square} = \bar{\boldsymbol{\zeta}}. \quad (13)$$

However, it is desirable to interpret the condition (13)₂ in terms of only boundary values on Γ_{\square} , such that (13) is replaced by

$$\langle \mu \rangle_{\square} = \bar{\mu}, \quad \langle \langle \mu \mathbf{n} \rangle \rangle_{\square} = \bar{\boldsymbol{\zeta}}. \quad (14)$$

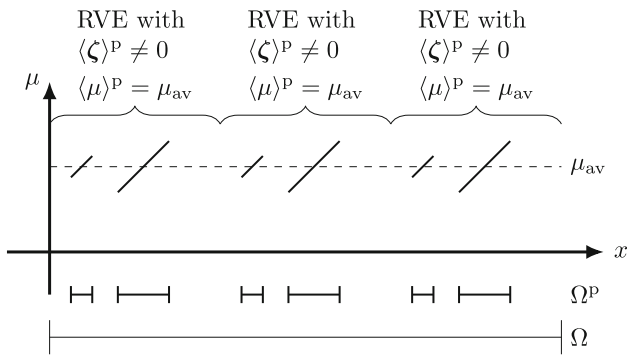


Fig. 2 Illustration of a fine-scale field in disjunct particles in a one dimensional space. Three adjacent RVEs are marked which all have the same average potential and non-zero average potential gradients

Now, due to the possibility of a jump of μ across Γ_{\square}^i , it appears that (13)₂ and (14)₂ are not equivalent. In fact, according to the definition in (1c), $\langle \zeta[\mu] \rangle_{\square} = \langle \zeta[\mu] \rangle_{\square}^p + \langle \zeta[\mu] \rangle_{\square}^m$, whereas it holds that

$$\langle \langle \mu \mathbf{n} \rangle \rangle_{\square} = \langle \zeta[\mu] \rangle_{\square}^p + \langle \zeta[\mu] \rangle_{\square}^m + \langle \langle [\mu] \mathbf{n}^i \rangle \rangle_{\square}^i, \tag{15}$$

where $\mathbf{n}^i = \mathbf{n}^p$ in accordance with the definition of the jump. Formally, we may express (14) as

$$\bar{\mu}_{\square}(\mu) = \bar{\mu}, \quad \bar{\zeta}_{\square}(\mu) = \bar{\zeta}, \tag{16}$$

in terms of the homogenization operators

$$\bar{\mu}_{\square}(\mu) := \langle \mu \rangle_{\square}, \tag{17a}$$

$$\bar{\zeta}_{\square}(\mu) := \langle \langle \mu \mathbf{n} \rangle \rangle_{\square} = \langle \zeta[\mu] \rangle_{\square}^p + \langle \zeta[\mu] \rangle_{\square}^m + \langle \langle [\mu] \mathbf{n}^i \rangle \rangle_{\square}^i. \tag{17b}$$

As to the boundary conditions on the RVE, the sub-scale fluctuation field μ^s is assumed periodic. For a mirror point $\mathbf{x} \in \Gamma_{\square}^+$ and the corresponding image point $\mathbf{x}^-(\mathbf{x}) \in \Gamma_{\square} \setminus \Gamma_{\square}^+$, cf. Figure 3, we define the RVE jump operator $\langle \langle \bullet \rangle \rangle_{\square}(\mathbf{x}) := \bullet(\mathbf{x}) - \bullet(\mathbf{x}^-(\mathbf{x}))$. Periodicity can then be described in the strong form as

$$\langle \langle \mu^s \rangle \rangle_{\square}(\mathbf{x}) = 0 \quad \forall \mathbf{x} \in \Gamma_{\square}^+. \tag{18}$$

This condition can be enforced in the weak form and applied using the Lagrange multiplier method as

$$\frac{1}{|\Omega_{\square}|} \int_{\Gamma_{\square}^+} \delta \lambda \langle \langle \mu \rangle \rangle_{\square} d\Gamma = \frac{1}{|\Omega_{\square}|} \int_{\Gamma_{\square}^+} \delta \lambda \langle \langle \mathbf{x} \rangle \rangle_{\square} d\Gamma \cdot \bar{\zeta} \quad \forall \delta \lambda \in \mathbb{J}_{\square}. \tag{19}$$

However, it can be shown that this condition is sufficiently general to incorporate (14)₂ as a special case. To show this,

we choose $\delta \lambda = \delta \bar{\lambda} \cdot \mathbf{n}$ with $\delta \bar{\lambda} \in \mathbb{R}^3$, whereby (19) becomes

$$\delta \bar{\lambda} \cdot \frac{1}{|\Omega_{\square}|} \int_{\Gamma_{\square}^+} \mu \mathbf{n} d\Gamma = \delta \bar{\lambda} \cdot \bar{\zeta} \quad \forall \delta \bar{\lambda} \in \mathbb{R}^3. \tag{20}$$

which is identical to (14)₂.

In conclusion, the RVE-problem reads: For given $\bar{\mu}(t)$, $\bar{\zeta}(t)$, find $\mu(\bullet, t) \in \mathbb{M}_{\square}$, $\bar{\lambda}_{\mu} \in \mathbb{R}$, $\lambda \in \mathbb{J}_{\square}$, that solve

$$\langle \partial_{t,c} \delta \mu \rangle_{\square} - \langle \mathbf{j}(\zeta[\mu]) \cdot \zeta[\delta \mu] \rangle_{\square} - \langle \langle j_n([\mu]) \rangle \rangle_{\square} \langle \langle \delta \mu \rangle \rangle_{\square}^i + \bar{\lambda}_{\mu} \langle \delta \mu \rangle_{\square} + \frac{1}{|\Omega_{\square}|} \int_{\Gamma_{\square}^+} \lambda \langle \langle \delta \mu \rangle \rangle_{\square} d\Gamma = 0$$

$$\forall \delta \mu \in \mathbb{M}_{\square}, \tag{21a}$$

$$\delta \bar{\lambda}_{\mu} \langle \mu \rangle_{\square} = \delta \bar{\lambda}_{\mu} \bar{\mu} \quad \forall \delta \bar{\lambda}_{\mu} \in \mathbb{R}, \tag{21b}$$

$$\frac{1}{|\Omega_{\square}|} \int_{\Gamma_{\square}^+} \delta \lambda \langle \langle \mu \rangle \rangle_{\square} d\Gamma = \frac{1}{|\Omega_{\square}|} \int_{\Gamma_{\square}^+} \delta \lambda \langle \langle \mathbf{x} \rangle \rangle_{\square} d\Gamma \cdot \bar{\zeta} \quad \forall \delta \lambda \in \mathbb{J}_{\square}. \tag{21c}$$

3.2.3 RVE-problem for moment-based constraints

An alternative to the gradient-based format are constraints in terms of 0th and 1st order moments of the fine-scale potential μ . By inspection, we conclude that

$$\langle \mu^M \rangle_{\square} = \bar{\mu}, \quad \langle \mu^M [\mathbf{x} - \bar{\mathbf{x}}] \rangle_{\square} = \bar{\zeta} \cdot \mathbf{X}, \tag{22}$$

where $\mathbf{X} := \langle [\mathbf{x} - \bar{\mathbf{x}}] \otimes [\mathbf{x} - \bar{\mathbf{x}}] \rangle_{\square}$ is the 2nd order tensor expressing moment of inertia. The appropriate constraints thus read

$$\langle \mu \rangle_{\square} = \bar{\mu}, \quad \langle \mu [\mathbf{x} - \bar{\mathbf{x}}] \rangle_{\square} = \bar{\zeta} \cdot \mathbf{X}. \tag{23}$$

Like for the gradient-based description, we may introduce the homogenization operators

$$\bar{\mu}_{\square}(\mu) := \langle \mu \rangle_{\square}, \tag{24a}$$

$$\bar{\zeta}_{\square}(\mu) := \langle \mu [\mathbf{x} - \bar{\mathbf{x}}] \rangle_{\square} \cdot \mathbf{X}^{-1}, \tag{24b}$$

whereby the constraints can be expressed precisely as in (16).

Finally, the RVE-problem reads: For given $\bar{\mu}(t)$, $\bar{\zeta}(t)$, find $\mu(\bullet, t) \in \mathbb{M}_{\square}$, $\bar{\lambda}_{\mu} \in \mathbb{R}$, $\bar{\lambda}_{\zeta} \in \mathbb{R}^3$, $\lambda \in \mathbb{J}_{\square}$, that solve

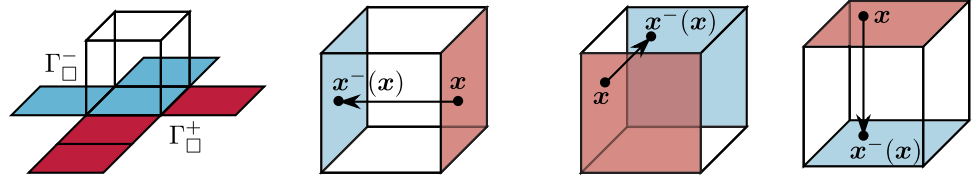
$$\langle \partial_{t,c} \delta \mu \rangle_{\square} - \langle \mathbf{j}(\zeta[\mu]) \cdot \zeta[\delta \mu] \rangle_{\square} - \langle \langle j_n([\mu]) \rangle \rangle_{\square} \langle \langle \delta \mu \rangle \rangle_{\square}^i + \bar{\lambda}_{\mu} \langle \delta \mu \rangle_{\square} + \bar{\lambda}_{\zeta} \cdot \langle \mu [\mathbf{x} - \bar{\mathbf{x}}] \rangle_{\square} + \frac{1}{|\Omega_{\square}|} \int_{\Gamma_{\square}^+} \lambda \langle \langle \delta \mu \rangle \rangle_{\square} d\Gamma = 0 \quad \forall \delta \mu \in \mathbb{M}_{\square}, \tag{25a}$$

$$\delta \bar{\lambda}_{\mu} \langle \mu \rangle_{\square} = \delta \bar{\lambda}_{\mu} \bar{\mu} \quad \forall \delta \bar{\lambda}_{\mu} \in \mathbb{R}, \tag{25b}$$

$$\delta \bar{\lambda}_{\zeta} \cdot \langle \mu [\mathbf{x} - \bar{\mathbf{x}}] \rangle_{\square} = \delta \bar{\lambda}_{\zeta} \cdot \langle \bar{\zeta} \cdot \mathbf{X} \rangle \quad \forall \delta \bar{\lambda}_{\zeta} \in \mathbb{R}^3, \tag{25c}$$

$$\frac{1}{|\Omega_{\square}|} \int_{\Gamma_{\square}^+} \delta \lambda \langle \langle \mu \rangle \rangle_{\square} d\Gamma = \frac{1}{|\Omega_{\square}|} \int_{\Gamma_{\square}^+} \delta \lambda \langle \langle \mathbf{x} \rangle \rangle_{\square} d\Gamma \cdot \bar{\zeta} \quad \forall \delta \lambda \in \mathbb{J}_{\square}. \tag{25d}$$

Fig. 3 Mirror and image RVE boundaries



Remark 1 This formulation of the single potential approach is not investigated further in this paper. However, it is used for the dual potential approach presented subsequently, which is the focus of this contribution.

4 Variationally consistent homogenization - dual potential approach

4.1 Preliminaries

Like for the single potential approach, we introduce running averages and decompose the chemical potential into macroscale contribution and sub-scale fluctuation. In contrast to (8), we propose to use a definition of μ^M based on one independent macroscale field per phase: $\bar{\mu}^P \in \bar{M}^P$ for the particles and $\bar{\mu}^m \in \bar{M}^m$ for the matrix. We shall adopt two different prolongations in what follows:

- Constant (0th order) prolongation of $\bar{\mu}^P$ for the particles and linear (1st order) prolongation of $\bar{\mu}^m$ for the matrix.
- Linear (1st order) prolongation of both $\bar{\mu}^P$ and $\bar{\mu}^m$.

For any linearly prolonged field, we may employ both the *gradient-based* and the *moment-based* approach to homogenization constraints. Note that we still consider a single potential μ on the sub-scale.

The presented dual potential approach is designed for cases with a low mobility across the interface or very low mobility inside the particles. In this case, we expect that the transport through the RVE is not significantly affected by flux through individual particles. For this reason, the constant-linear prolongation is investigated, which neglects the corresponding part of the overall flux. Moreover, this motivates the application of moment-based constraints when using a linear-linear prolongation. This way, the gradient of $\bar{\mu}^P$ results in potential differences between particles rather than gradients inside individual particles. Besides these two methods, the linear-linear prolongation with gradient-based constraints is used for a comparison.

4.2 Constant-linear prolongation

Applying a constant prolongation of $\bar{\mu}^P \in \bar{M}^P$ and a linear prolongation of $\bar{\mu}^m \in \bar{M}^m$ results in

$$\mu^M[\bar{\mu}^P, \bar{\mu}^m](\bar{x}, x) = \begin{cases} \bar{\mu}^P(\bar{x}) & , x \in \Omega_{\square}^P \\ \bar{\mu}^m(\bar{x}) + \bar{\xi}^m(\bar{x}) \cdot [x - \bar{x}] & , x \in \Omega_{\square}^m \end{cases}, \quad (26)$$

where $\bar{\xi}^m := \nabla \bar{\mu}^m$.

In analogy with the developments for the single macroscale potential, the two-scale problem is derived from (6) upon inserting (7) and (26): For given $\mu^{\text{pre}}(t)$, $j_n^{\text{pre}}(t)$, find $\bar{\mu}^P(\bullet, t) \in \bar{M}^P$, $\bar{\mu}^m(\bullet, t) \in \bar{M}^m$, $\mu^s(\bullet, t) \in \bar{M}^s$, that solve

$$\begin{aligned} & \int_{\Omega} \langle \partial_t c [\mu^M[\delta \bar{\mu}^P, \delta \bar{\mu}^m] + \delta \mu^s] \rangle_{\square} d\Omega \\ & - \int_{\Omega} \langle j \left(\bar{\xi} [\mu^M[\bar{\mu}^P, \bar{\mu}^m] + \mu^s] \right) \cdot \bar{\xi} [\mu^M[\delta \bar{\mu}^P, \delta \bar{\mu}^m] + \delta \mu^s] \rangle_{\square} d\Omega \\ & - \int_{\Omega} \langle \langle j_n \left(\llbracket \mu^M[\bar{\mu}^P, \bar{\mu}^m] + \mu^s \rrbracket \right) \llbracket \mu^M[\delta \bar{\mu}^P, \delta \bar{\mu}^m] + \delta \mu^s \rrbracket \rangle_{\square}^i \rangle d\Omega \\ & = \int_{\Gamma_N} -j_n^{\text{pre}} [\mu^M[\delta \bar{\mu}^P, \delta \bar{\mu}^m] + \delta \mu^s] d\Gamma \\ & \quad \forall (\delta \bar{\mu}^P, \delta \bar{\mu}^m, \delta \mu^s) \in \bar{M}^{P,0} \times \bar{M}^{m,0} \times \bar{M}^{s,0}. \end{aligned} \quad (27)$$

With the definition $\delta \bar{\xi}^m := \nabla \delta \bar{\mu}^m$, the macroscale problem reads: For given $\bar{\mu}^{m,\text{pre}}(t)$, $\bar{j}_n^{m,\text{pre}}(t)$, find $\bar{\mu}^P(\bullet, t) \in \bar{M}^P$, $\bar{\mu}^m(\bullet, t) \in \bar{M}^m$, that solve

$$\begin{aligned} & \int_{\Omega} \partial_t \bar{c}^P \delta \bar{\mu}^P + \bar{r} \delta \bar{\mu}^P d\Omega = 0 \\ & \quad \forall \delta \bar{\mu}^P \in \bar{M}^{P,0}, \end{aligned} \quad (28a)$$

$$\begin{aligned} & \int_{\Omega} \partial_t \bar{c}^m \delta \bar{\mu}^m - (\bar{j}^m - \partial_t \bar{c}_2^m + \bar{r}_2) \cdot \delta \bar{\xi}^m - \bar{r} \delta \bar{\mu}^m d\Omega \\ & = \int_{\Gamma_N^m} -\bar{j}_n^{m,\text{pre}} \delta \bar{\mu}^m d\Gamma \\ & \quad \forall \delta \bar{\mu}^m \in \bar{M}^{m,0}, \end{aligned} \quad (28b)$$

where the homogenized fields are given as

$$\bar{c}^P := \langle c \rangle_{\square}^P, \quad (29a)$$

$$\bar{c}^m := \langle c \rangle_{\square}^m, \quad \bar{c}_2^m := \langle c[x - \bar{x}] \rangle_{\square}^m, \quad (29b)$$

$$\bar{j}^m := \langle j \rangle_{\square}^m, \tag{29c}$$

$$\bar{r} := \langle \langle j_n \rangle \rangle_{\square}^i, \quad \bar{r}_2 := \langle \langle j_n [x - \bar{x}] \rangle \rangle_{\square}^i. \tag{29d}$$

The function spaces are defined as

$$\bar{M}^P = \bar{M}^{P,0} = \mathbb{L}_2(\Omega), \tag{30a}$$

$$\bar{M}^m = \{ \mu \in \mathbb{H}^1(\Omega) : \mu|_{\Gamma_D^m} = \bar{\mu}^{m,pre} \}, \tag{30b}$$

$$\bar{M}^{m,0} = \{ \mu \in \mathbb{H}^1(\Omega) : \mu|_{\Gamma_D^m} = 0 \}, \tag{30c}$$

where $\mathbb{L}_2(\bullet)$ is the space of square integrable functions. Compared to (10) for the single potential approach, the additional terms \bar{r} and \bar{r}_2 explicitly account for the transport across the interface.

Remark 2 According to (28a), \bar{c}^P is a local quantity and is itself not subject to any macroscopic diffusion equation.

Remark 3 The strong form of the problem reads: For given $\bar{\mu}^{m,pre}(t)$, $\bar{j}_n^{m,pre}(t)$, find $\bar{\mu}^P(x, t)$, $\bar{\mu}^m(x, t)$, that solve

$$\partial_t \bar{c}^P + \bar{r} = 0 \tag{31a}$$

in $\Omega \times (0, T]$,

$$\partial_t \bar{c}^m + (\bar{j}^m - \partial_t \bar{c}_2^m + \bar{r}_2) \cdot \nabla - \bar{r} = 0 \tag{31b}$$

in $\Omega \times (0, T]$,

$$\bar{\mu}^m = \bar{\mu}^{m,pre} \tag{31c}$$

on $\Gamma_D^m \times (0, T]$,

$$(\bar{j}^m - \partial_t \bar{c}_2^m + \bar{r}_2) \cdot n = \bar{j}_n^{m,pre} \tag{31d}$$

on $\Gamma_N^m \times (0, T]$.

4.2.1 RVE-problem for moment-based constraints

Extending the approach taken for the single potential leading to (23), we choose homogenization constraints as

$$\langle \mu \rangle^P = \bar{\mu}^P, \tag{32a}$$

$$\langle \mu \rangle^m = \bar{\mu}^m + \bar{\xi}^m \cdot \langle (x)^m - \bar{x} \rangle, \tag{32b}$$

$$\langle \mu [x - \bar{x}] \rangle^m = \bar{\xi}^m \cdot \langle [x - \bar{x}] \otimes [x - \bar{x}] \rangle^m + \bar{\mu}^m \langle (x)^m - \bar{x} \rangle, \tag{32c}$$

which are satisfied for $\mu = \mu^M$. It is possible to establish homogenization operators, $\bar{\mu}_{\square}^P(\mu)$, $\bar{\mu}_{\square}^m(\mu)$, and $\bar{\xi}_{\square}^m(\mu)$, such that (32) can be rephrased in the same canonical format as for the single potential approach in (16):

$$\bar{\mu}_{\square}^P(\mu) = \bar{\mu}^P, \tag{33a}$$

$$\bar{\mu}_{\square}^m(\mu) = \bar{\mu}^m, \tag{33b}$$

$$\bar{\xi}_{\square}^m(\mu) = \bar{\xi}^m. \tag{33c}$$

The homogenization operators can be expressed as

$$\bar{\mu}_{\square}^P(\mu) = \langle \mu \rangle^P, \tag{34a}$$

$$\bar{\mu}_{\square}^m(\mu) = \frac{1}{1 - \bar{x}^m \cdot [X^m]^{-1} \cdot \bar{x}^m} \left[\langle \mu \rangle^m - \bar{x}^m \cdot [X^m]^{-1} \cdot \langle \mu [x - \bar{x}] \rangle^m \right], \tag{34b}$$

$$\bar{\xi}_{\square}^m(\mu) = \left[[X^m]^{-1} + \frac{\bar{x}^m \cdot [X^m]^{-1} \otimes \bar{x}^m \cdot [X^m]^{-1}}{1 - \bar{x}^m \cdot [X^m]^{-1} \cdot \bar{x}^m} \right] \cdot \langle \mu [x - \bar{x}] \rangle^m - \frac{\bar{x}^m \cdot [X^m]^{-1}}{1 - \bar{x}^m \cdot [X^m]^{-1} \cdot \bar{x}^m} \langle \mu \rangle^m, \tag{34c}$$

where we introduce the notation $\bar{x}^m := \langle x \rangle^m - \bar{x}$, $X^m := \langle [x - \bar{x}] \otimes [x - \bar{x}] \rangle^m$. Note that \bar{x}^m vanishes, when the RVE is large enough, and the definitions simplify.

Remark 4 Once again, we note that the operational form of the homogenization constraints is that given in (32). The canonical form in (33) shows merely that it is possible to construct the operators in (34) in a unique fashion.

The transient RVE-problem for periodic boundary conditions, derived from (27) by choosing $\delta \bar{\mu}^P = \delta \bar{\mu}^m = 0$, reads: For given $\bar{\mu}^P(t)$, $\bar{\mu}^m(t)$, $\bar{\xi}^m(t)$, find $\mu(\bullet, t) \in \mathbb{M}_{\square}$, $\bar{\lambda}_{\mu}^P(t) \in \mathbb{R}$, $\bar{\lambda}_{\mu}^m(t) \in \mathbb{R}$, $\bar{\lambda}_{\xi}^m(t) \in \mathbb{R}^3$, $\lambda(t) \in \mathbb{J}_{\square}$, that solve

$$\langle \partial_t c \delta \mu \rangle_{\square} - \langle j(\xi[\mu]) \cdot \xi[\delta \mu] \rangle_{\square} - \langle \langle j_n(\llbracket \mu \rrbracket) \llbracket \delta \mu \rrbracket \rangle \rangle_{\square}^i + \bar{\lambda}_{\mu}^P \langle \delta \mu \rangle^P + \bar{\lambda}_{\mu}^m \langle \delta \mu \rangle^m + \bar{\lambda}_{\xi}^m \cdot \langle \delta \mu [x - \bar{x}] \rangle^m + \frac{1}{|\Omega_{\square}|} \int_{\Gamma_{\square}^+} \lambda \llbracket \delta \mu \rrbracket_{\square} d\Gamma = 0 \tag{35a}$$

$\forall \delta \mu \in \mathbb{M}_{\square}$,

$$\delta \bar{\lambda}_{\mu}^P \langle \mu \rangle^P = \delta \bar{\lambda}_{\mu}^P \bar{\mu}^P \tag{35b}$$

$\forall \delta \bar{\lambda}_{\mu}^P \in \mathbb{R}$,

$$\delta \bar{\lambda}_{\mu}^m \langle \mu \rangle^m = \delta \bar{\lambda}_{\mu}^m [\bar{\mu}^m + \bar{\xi}^m \cdot \langle (x)^m - \bar{x} \rangle] \tag{35c}$$

$\forall \delta \bar{\lambda}_{\mu}^m \in \mathbb{R}$,

$$\delta \bar{\lambda}_{\xi}^m \cdot \langle \mu [x - \bar{x}] \rangle^m = \delta \bar{\lambda}_{\xi}^m \cdot \left[\bar{\xi}^m \cdot \langle [x - \bar{x}] \otimes [x - \bar{x}] \rangle^m + [\bar{\mu}^m \langle (x)^m - \bar{x} \rangle] \right] \tag{35d}$$

$\forall \delta \bar{\lambda}_{\xi}^m \in \mathbb{R}^3$,

$$\frac{1}{|\Omega_{\square}|} \int_{\Gamma_{\square}^+} \delta \lambda \llbracket \mu \rrbracket_{\square} d\Gamma = \frac{1}{|\Omega_{\square}|} \int_{\Gamma_{\square}^{m+}} \delta \lambda \llbracket x \rrbracket_{\square} d\Gamma \cdot \bar{\xi}^m \tag{35e}$$

$\forall \delta \lambda \in \mathbb{J}_{\square}$,

where we introduced the RVE solution and test function spaces

$$\mathbb{M}_{\square} = \{ \mu \in \mathbb{L}_2(\Omega_{\square}^P \cup \Omega_{\square}^m) : \mu|_{\Gamma_i} \in \mathbb{H}^1(\Gamma_i) \}, \tag{36a}$$

$$\mathbb{J}_{\square} = \mathbb{L}_2(\Gamma_{\square}^+). \tag{36b}$$

Remark 5 Choosing $\delta \mu \in \mathbb{R}$, we obtain $\bar{\lambda}_{\mu}^P + \bar{\lambda}_{\mu}^m = -\langle \partial_t c \rangle_{\square}$ from (35a). Further, it is possible to show that λ represent self-equilibrated normal fluxes on the RVE boundary [21].

Remark 6 It can be shown that the variationally consistent macro-homogeneity condition (or generalized Hill-Mandel condition) is satisfied. Details are given in Appendix A.

4.3 Linear-linear prolongation

Linear prolongation can be assumed for both macroscale potentials $\bar{\mu}^p$ and $\bar{\mu}^m$, i.e.

$$\mu^M[\bar{\mu}^p, \bar{\mu}^m](\bar{x}, \mathbf{x}) = \begin{cases} \bar{\mu}^p(\bar{x}) + \bar{\xi}^p(\bar{x}) \cdot [\mathbf{x} - \bar{x}] & , \mathbf{x} \in \Omega_{\square}^p \\ \bar{\mu}^m(\bar{x}) + \bar{\xi}^m(\bar{x}) \cdot [\mathbf{x} - \bar{x}] & , \mathbf{x} \in \Omega_{\square}^m \end{cases}, \tag{37}$$

where $\bar{\xi}^p := \nabla \bar{\mu}^p$ and $\bar{\xi}^m := \nabla \bar{\mu}^m$. With the definitions $\delta \bar{\xi}^p := \nabla \delta \bar{\mu}^p$, $\bar{c}_2^p := \langle c[\mathbf{x} - \bar{x}] \rangle_{\square}^p$ and $\bar{j}^p := \langle \mathbf{j} \rangle_{\square}^p$, the corresponding macroscale problem reads: For given $\bar{\mu}^{p,pre}(t)$, $\bar{j}_n^{p,pre}(t)$, $\bar{\mu}^{m,pre}(t)$, $\bar{j}_n^{m,pre}(t)$, find $\bar{\mu}^p(\bullet, t) \in \bar{M}^p$, $\bar{\mu}^m(\bullet, t) \in \bar{M}^m$, that solve

$$\begin{aligned} & \int_{\Omega} \partial_t \bar{c}^p \delta \bar{\mu}^p - [\bar{j}^p - \partial_t \bar{c}_2^p - \bar{r}_2] \cdot \delta \bar{\xi}^p + \bar{r} \delta \bar{\mu}^p d\Omega \\ & = \int_{\Gamma_N^p} -\bar{j}_n^{p,pre} \delta \bar{\mu}^p d\Gamma \\ & \quad \forall \delta \bar{\mu}^p \in \bar{M}^{p,0}, \end{aligned} \tag{38a}$$

$$\begin{aligned} & \int_{\Omega} \partial_t \bar{c}^m \delta \bar{\mu}^m - [\bar{j}^m - \partial_t \bar{c}_2^m + \bar{r}_2] \cdot \delta \bar{\xi}^m - \bar{r} \delta \bar{\mu}^m d\Omega \\ & = \int_{\Gamma_N^m} -\bar{j}_n^{m,pre} \delta \bar{\mu}^m d\Gamma \\ & \quad \forall \delta \bar{\mu}^m \in \bar{M}^{m,0}. \end{aligned} \tag{38b}$$

The solution and test function spaces are defined as

$$\bar{M}^p = \{ \mu \in H^1(\Omega) : \mu|_{\Gamma_D^p} = \bar{\mu}^{p,pre} \}, \tag{39a}$$

$$\bar{M}^{p,0} = \{ \mu \in H^1(\Omega) : \mu|_{\Gamma_D^p} = 0 \}, \tag{39b}$$

$$\bar{M}^m = \{ \mu \in H^1(\Omega) : \mu|_{\Gamma_D^m} = \bar{\mu}^{m,pre} \}, \tag{39c}$$

$$\bar{M}^{m,0} = \{ \mu \in H^1(\Omega) : \mu|_{\Gamma_D^m} = 0 \}. \tag{39d}$$

Remark 7 Compared to the macroscale model using a constant-linear prolongation, the model in (38) contains the gradient $\bar{\xi}^p$. This enriches the model; making it more versatile, but also more complex.

Remark 8 The strong form of the problem reads: For given $\bar{\mu}^{m,pre}(t)$, $\bar{j}_n^{m,pre}(t)$, find $\bar{\mu}^p(\mathbf{x}, t)$, $\bar{\mu}^m(\mathbf{x}, t)$, that solve

$$\begin{aligned} & \partial_t \bar{c}^p + (\bar{j}^p - \partial_t \bar{c}_2^p - \bar{r}_2) \cdot \nabla + \bar{r} = 0 \\ & \quad \text{in } \Omega \times (0, T], \end{aligned} \tag{40a}$$

$$\partial_t \bar{c}^m + (\bar{j}^m - \partial_t \bar{c}_2^m + \bar{r}_2) \cdot \nabla - \bar{r} = 0$$

$$\text{in } \Omega \times (0, T], \tag{40b}$$

$$\begin{aligned} & \bar{\mu}^p = \bar{\mu}^{p,pre} \\ & \quad \text{on } \Gamma_D^p \times (0, T], \end{aligned} \tag{40c}$$

$$\begin{aligned} & \bar{\mu}^m = \bar{\mu}^{m,pre} \\ & \quad \text{on } \Gamma_D^m \times (0, T], \end{aligned} \tag{40d}$$

$$\begin{aligned} & (\bar{j}^p - \partial_t \bar{c}_2^p - \bar{r}_2) \cdot \mathbf{n} = \bar{j}_n^{p,pre} \\ & \quad \text{on } \Gamma_N^p \times (0, T], \end{aligned} \tag{40e}$$

$$\begin{aligned} & (\bar{j}^m - \partial_t \bar{c}_2^m + \bar{r}_2) \cdot \mathbf{n} = \bar{j}_n^{m,pre} \\ & \quad \text{on } \Gamma_N^m \times (0, T]. \end{aligned} \tag{40f}$$

4.3.1 RVE-problem for gradient-based constraints

We introduce gradient-based homogenization constraints for both fields as

$$\langle \mu \rangle^p = \bar{\mu}^p + \langle \xi[\mu] \rangle^p \cdot [\langle \mathbf{x} \rangle^p - \bar{x}], \tag{41a}$$

$$\langle \xi[\mu] \rangle^p = \bar{\xi}^p, \tag{41b}$$

$$\langle \mu \rangle^m = \bar{\mu}^m + \langle \xi[\mu] \rangle^m \cdot [\langle \mathbf{x} \rangle^m - \bar{x}], \tag{41c}$$

$$\langle \xi[\mu] \rangle^m = \bar{\xi}^m, \tag{41d}$$

which are satisfied for $\mu = \mu^M$. Once again, it is possible to establish homogenization operators, $\bar{\mu}_{\square}^p(\mu)$, $\bar{\mu}_{\square}^m(\mu)$, $\bar{\xi}_{\square}^p(\mu)$ and $\bar{\xi}_{\square}^m(\mu)$, such that (41) can be rephrased in the canonical form

$$\bar{\mu}_{\square}^p(\mu) = \bar{\mu}^p, \tag{42a}$$

$$\bar{\xi}_{\square}^p(\mu) = \bar{\xi}^p, \tag{42b}$$

$$\bar{\mu}_{\square}^m(\mu) = \bar{\mu}^m, \tag{42c}$$

$$\bar{\xi}_{\square}^m(\mu) = \bar{\xi}^m. \tag{42d}$$

Now, we introduce the quantities $(\bar{x}^p, \mathbf{X}^p)$ in complete analogy with $(\bar{x}^m, \mathbf{X}^m)$. The homogenization operators can then be expressed as

$$\bar{\mu}_{\square}^p(\mu) = \langle \mu \rangle^p - \langle \xi[\mu] \rangle^p \cdot \bar{x}^p, \tag{43a}$$

$$\bar{\xi}_{\square}^p(\mu) = \langle \xi[\mu] \rangle^p, \tag{43b}$$

$$\bar{\mu}_{\square}^m(\mu) = \langle \mu \rangle^m - \langle \xi[\mu] \rangle^m \cdot \bar{x}^m, \tag{43c}$$

$$\bar{\xi}_{\square}^m(\mu) = \langle \xi[\mu] \rangle^m. \tag{43d}$$

Finally, the RVE-problem reads: For given $\bar{\mu}^p(t)$, $\bar{\xi}^p(t)$, $\bar{\mu}^m(t)$, $\bar{\xi}^m(t)$, find $\mu(\bullet, t) \in M_{\square}$, $\bar{\lambda}_{\mu}^p(t) \in \mathbb{R}$, $\bar{\lambda}_{\mu}^m(t) \in \mathbb{R}$, $\bar{\lambda}_{\xi}^p(t) \in \mathbb{R}^3$, $\bar{\lambda}_{\xi}^m(t) \in \mathbb{R}^3$, $\lambda(t) \in \mathbb{J}_{\square}$, that solve

$$\begin{aligned} & \langle \partial_t c \delta \mu \rangle_{\square} - \langle \mathbf{j}(\xi[\mu]) \cdot \xi[\delta \mu] \rangle_{\square} - \langle j_n(\llbracket \mu \rrbracket) \llbracket \delta \mu \rrbracket \rangle_{\square} \\ & \quad + \bar{\lambda}_{\mu}^p \langle \delta \mu \rangle^p + \bar{\lambda}_{\mu}^m \langle \delta \mu \rangle^m + \bar{\lambda}_{\xi}^p \cdot \langle \delta \xi[\delta \mu] \rangle^p + \bar{\lambda}_{\xi}^m \cdot \langle \delta \xi[\delta \mu] \rangle^m \\ & \quad + \frac{1}{|\Omega_{\square}|} \int_{\Gamma_{\square}^+} \lambda \llbracket \delta \mu \rrbracket d\Gamma = 0 \end{aligned}$$

$$\forall \delta \mu \in \mathbb{M}_{\square}, \tag{44a}$$

$$\delta \bar{\lambda}_{\mu}^p \langle \mu \rangle^p = \delta \bar{\lambda}_{\mu}^p [\bar{\mu}^p + \bar{\xi}^p \cdot \langle (x)^p - \bar{x} \rangle] \tag{44b}$$

$$\forall \delta \bar{\lambda}_{\mu}^p \in \mathbb{R},$$

$$\delta \bar{\lambda}_{\mu}^m \langle \mu \rangle^m = \delta \bar{\lambda}_{\mu}^m [\bar{\mu}^m + \bar{\xi}^m \cdot \langle (x)^m - \bar{x} \rangle] \tag{44c}$$

$$\forall \delta \bar{\lambda}_{\mu}^m \in \mathbb{R},$$

$$\delta \bar{\lambda}_{\zeta}^p \cdot \langle \zeta[\mu] \rangle^p = \delta \bar{\lambda}_{\zeta}^p \cdot \bar{\xi}^p \tag{44d}$$

$$\forall \delta \bar{\lambda}_{\zeta}^p \in \mathbb{R}^3,$$

$$\delta \bar{\lambda}_{\zeta}^m \cdot \langle \zeta[\mu] \rangle^m = \delta \bar{\lambda}_{\zeta}^m \cdot \bar{\xi}^m \tag{44e}$$

$$\forall \delta \bar{\lambda}_{\zeta}^m \in \mathbb{R}^3,$$

$$\frac{1}{|\Omega_{\square}|} \int_{\Gamma_{\square}^+} \delta \lambda \llbracket \mu \rrbracket_{\square} d\Gamma = \frac{1}{|\Omega_{\square}|} \int_{\Gamma_{\square}^{p+}} \delta \lambda \llbracket x \rrbracket_{\square} d\Gamma \cdot \bar{\xi}^p \tag{44f}$$

$$+ \frac{1}{|\Omega_{\square}|} \int_{\Gamma_{\square}^{m+}} \delta \lambda \llbracket x \rrbracket_{\square} d\Gamma \cdot \bar{\xi}^m \tag{44g}$$

$$\forall \delta \lambda \in \mathbb{J}_{\square}.$$

4.3.2 RVE-problem for moment-based constraints

Moment-based homogenization constraints for both fields can be expressed as

$$\langle \mu \rangle^p = \bar{\mu}^p + \bar{\xi}^p \cdot \langle (x)^p - \bar{x} \rangle, \tag{45a}$$

$$\langle \mu [x - \bar{x}] \rangle^p = \bar{\xi}^p \cdot \langle [x - \bar{x}] \otimes [x - \bar{x}] \rangle^p + \bar{\mu}^p \langle (x)^p - \bar{x} \rangle, \tag{45b}$$

$$\langle \mu \rangle^m = \bar{\mu}^m + \bar{\xi}^m \cdot \langle (x)^m - \bar{x} \rangle, \tag{45c}$$

$$\langle \mu [x - \bar{x}] \rangle^m = \bar{\xi}^m \cdot \langle [x - \bar{x}] \otimes [x - \bar{x}] \rangle^m + \bar{\mu}^m \langle (x)^m - \bar{x} \rangle, \tag{45d}$$

which are satisfied for $\mu = \mu^M$. It is possible to establish homogenization operators, such that (45) can be rephrased in the canonical form that was given already in (42). These operators are defined as

$$\bar{\mu}_{\square}^p(\mu) = \frac{1}{1 - \bar{x}^p \cdot [X^p]^{-1} \cdot \bar{x}^p} \left[\langle \mu \rangle^p - \bar{x}^p \cdot [X^p]^{-1} \cdot \langle \mu [x - \bar{x}] \rangle^p \right], \tag{46a}$$

$$\bar{\xi}_{\square}^p(\mu) = \left[[X^p]^{-1} + \frac{\bar{x}^p \cdot [X^p]^{-1} \otimes \bar{x}^p \cdot [X^p]^{-1}}{1 - \bar{x}^p \cdot [X^p]^{-1} \cdot \bar{x}^p} \right] \cdot \langle \mu [x - \bar{x}] \rangle^p - \frac{\bar{x}^p \cdot [X^p]^{-1}}{1 - \bar{x}^p \cdot [X^p]^{-1} \cdot \bar{x}^p} \langle \mu \rangle^p, \tag{46b}$$

$$\bar{\mu}_{\square}^m(\mu) = \frac{1}{1 - \bar{x}^m \cdot [X^m]^{-1} \cdot \bar{x}^m} \left[\langle \mu \rangle^m - \bar{x}^m \cdot [X^m]^{-1} \cdot \langle \mu [x - \bar{x}] \rangle^m \right], \tag{46c}$$

$$\bar{\xi}_{\square}^m(\mu) = \left[[X^m]^{-1} + \frac{\bar{x}^m \cdot [X^m]^{-1} \otimes \bar{x}^m \cdot [X^m]^{-1}}{1 - \bar{x}^m \cdot [X^m]^{-1} \cdot \bar{x}^m} \right] \cdot \langle \mu [x - \bar{x}] \rangle^m.$$

$$\langle \mu [x - \bar{x}] \rangle^m - \frac{\bar{x}^m \cdot [X^m]^{-1}}{1 - \bar{x}^m \cdot [X^m]^{-1} \cdot \bar{x}^m} \langle \mu \rangle^m. \tag{46d}$$

The RVE-problem now becomes: For given $\bar{\mu}^p(t), \bar{\xi}^p(t), \bar{\mu}^m(t), \bar{\xi}^m(t)$, find $\mu(\bullet, t) \in \mathbb{M}_{\square}, \bar{\lambda}_{\mu}^p(t) \in \mathbb{R}, \bar{\lambda}_{\mu}^m(t) \in \mathbb{R}, \bar{\lambda}_{\zeta}^p(t) \in \mathbb{R}^3, \bar{\lambda}_{\zeta}^m(t) \in \mathbb{R}^3, \lambda(t) \in \mathbb{J}_{\square}$, that solve

$$\langle \partial_t c \delta \mu \rangle_{\square} - \langle j(\zeta[\mu]) \cdot \zeta[\delta \mu] \rangle_{\square} - \langle \langle j_n(\llbracket \mu \rrbracket) \llbracket \delta \mu \rrbracket \rangle \rangle_{\square}^i + \bar{\lambda}_{\mu}^p \langle \delta \mu \rangle^p + \bar{\lambda}_{\mu}^m \langle \delta \mu \rangle^m + \bar{\lambda}_{\zeta}^p \cdot \langle \delta \mu [x - \bar{x}] \rangle^p + \bar{\lambda}_{\zeta}^m \cdot \langle \delta \mu [x - \bar{x}] \rangle^m + \frac{1}{|\Omega_{\square}|} \int_{\Gamma_{\square}^+} \lambda \llbracket \delta \mu \rrbracket_{\square} d\Gamma = 0 \tag{47a}$$

$$\forall \delta \mu \in \mathbb{M}_{\square}, \tag{47a}$$

$$\delta \bar{\lambda}_{\mu}^p \langle \mu \rangle^p = \delta \bar{\lambda}_{\mu}^p [\bar{\mu}^p + \bar{\xi}^p \cdot \langle (x)^p - \bar{x} \rangle] \tag{47b}$$

$$\forall \delta \bar{\lambda}_{\mu}^p \in \mathbb{R},$$

$$\delta \bar{\lambda}_{\mu}^m \langle \mu \rangle^m = \delta \bar{\lambda}_{\mu}^m [\bar{\mu}^m + \bar{\xi}^m \cdot \langle (x)^m - \bar{x} \rangle] \tag{47c}$$

$$\forall \delta \bar{\lambda}_{\mu}^m \in \mathbb{R},$$

$$\delta \bar{\lambda}_{\zeta}^p \cdot \langle \mu [x - \bar{x}] \rangle^p = \delta \bar{\lambda}_{\zeta}^p \cdot \left[\bar{\xi}^p \cdot \langle [x - \bar{x}] \otimes [x - \bar{x}] \rangle^p + [\bar{\mu}^p \langle (x)^p - \bar{x} \rangle] \right] \tag{47d}$$

$$\forall \delta \bar{\lambda}_{\zeta}^p \in \mathbb{R}^3,$$

$$\delta \bar{\lambda}_{\zeta}^m \cdot \langle \mu [x - \bar{x}] \rangle^m = \delta \bar{\lambda}_{\zeta}^m \cdot \left[\bar{\xi}^m \cdot \langle [x - \bar{x}] \otimes [x - \bar{x}] \rangle^m + [\bar{\mu}^m \langle (x)^m - \bar{x} \rangle] \right] \tag{47e}$$

$$\forall \delta \bar{\lambda}_{\zeta}^m \in \mathbb{R}^3,$$

$$\frac{1}{|\Omega_{\square}|} \int_{\Gamma_{\square}^+} \delta \lambda \llbracket \mu \rrbracket_{\square} d\Gamma = \frac{1}{|\Omega_{\square}|} \int_{\Gamma_{\square}^{p+}} \delta \lambda \llbracket x \rrbracket_{\square} d\Gamma \cdot \bar{\xi}^p + \frac{1}{|\Omega_{\square}|} \int_{\Gamma_{\square}^{m+}} \delta \lambda \llbracket x \rrbracket_{\square} d\Gamma \cdot \bar{\xi}^m \tag{47f}$$

$$\forall \delta \lambda \in \mathbb{R}. \tag{47g}$$

5 Upscaling

We assume that both length and time scales (of RVE and macroscale problem) are sufficiently separated. In this case, the special situation of micro-stationarity is well motivated [23]: The RVE response adapts instantaneously to changes in the macroscopic data ($\bar{\mu}^p, \bar{\mu}^m, \bar{\xi}^p, \bar{\xi}^m$). Thus, the quantities in the transient macroscale problem can be computed from the solution of the stationary RVE-problem. Moreover, due to the linearity of the problem, the homogenized fields in the macroscale problems can be upscaled from the corresponding RVE-problem via superposition of sensitivity fields. These sensitivities can be obtained solving the stationary RVE-problem for unit load cases.

Subsequently, we present the upscaling scheme for the dual potential approach with a linear-linear prolongation. The procedures for the single potential approach and the dual potential approach with a constant-linear prolongation can be derived analogously.

Firstly, the chemical potential is additively decomposed as

$$\mu = \mu_l + \hat{\mu}_{\bar{\mu}^p} \bar{\mu}^p + \hat{\mu}_{\bar{\zeta}^p} \cdot \bar{\zeta}^p + \hat{\mu}_{\bar{\mu}^m} \bar{\mu}^m + \hat{\mu}_{\bar{\zeta}^m} \cdot \bar{\zeta}^m. \quad (48)$$

Secondly, a similar decomposition is introduced for all quantities which are relevant for the macroscale model:

$$\bar{c}^p = \bar{c}_l^p + \hat{c}_{\bar{\mu}^p}^p \bar{\mu}^p + \hat{c}_{\bar{\zeta}^p}^p \cdot \bar{\zeta}^p + \hat{c}_{\bar{\mu}^m}^p \bar{\mu}^m + \hat{c}_{\bar{\zeta}^m}^p \cdot \bar{\zeta}^m, \quad (49a)$$

$$\bar{c}^m = \bar{c}_l^m + \hat{c}_{\bar{\mu}^p}^m \bar{\mu}^p + \hat{c}_{\bar{\zeta}^p}^m \cdot \bar{\zeta}^p + \hat{c}_{\bar{\mu}^m}^m \bar{\mu}^m + \hat{c}_{\bar{\zeta}^m}^m \cdot \bar{\zeta}^m, \quad (49b)$$

$$\bar{c}_2^p = \bar{c}_{2,l}^p + \hat{c}_{2,\bar{\mu}^p}^p \bar{\mu}^p + \hat{c}_{2,\bar{\zeta}^p}^p \cdot \bar{\zeta}^p + \hat{c}_{2,\bar{\mu}^m}^p \bar{\mu}^m + \hat{c}_{2,\bar{\zeta}^m}^p \cdot \bar{\zeta}^m, \quad (49c)$$

$$\bar{c}_2^m = \bar{c}_{2,l}^m + \hat{c}_{2,\bar{\mu}^p}^m \bar{\mu}^p + \hat{c}_{2,\bar{\zeta}^p}^m \cdot \bar{\zeta}^p + \hat{c}_{2,\bar{\mu}^m}^m \bar{\mu}^m + \hat{c}_{2,\bar{\zeta}^m}^m \cdot \bar{\zeta}^m, \quad (49d)$$

$$\bar{j}^p = \bar{j}_l^p + \hat{j}_{\bar{\mu}^p}^p \bar{\mu}^p + \hat{j}_{\bar{\zeta}^p}^p \cdot \bar{\zeta}^p + \hat{j}_{\bar{\mu}^m}^p \bar{\mu}^m + \hat{j}_{\bar{\zeta}^m}^p \cdot \bar{\zeta}^m, \quad (49e)$$

$$\bar{j}^m = \bar{j}_l^m + \hat{j}_{\bar{\mu}^p}^m \bar{\mu}^p + \hat{j}_{\bar{\zeta}^p}^m \cdot \bar{\zeta}^p + \hat{j}_{\bar{\mu}^m}^m \bar{\mu}^m + \hat{j}_{\bar{\zeta}^m}^m \cdot \bar{\zeta}^m, \quad (49f)$$

$$\bar{r} = \bar{r}_l + \hat{r}_{\bar{\mu}^p} \bar{\mu}^p + \hat{r}_{\bar{\zeta}^p} \cdot \bar{\zeta}^p + \hat{r}_{\bar{\mu}^m} \bar{\mu}^m + \hat{r}_{\bar{\zeta}^m} \cdot \bar{\zeta}^m, \quad (49g)$$

$$\bar{r}_2 = \bar{r}_{2,l} + \hat{r}_{2,\bar{\mu}^p} \bar{\mu}^p + \hat{r}_{2,\bar{\zeta}^p} \cdot \bar{\zeta}^p + \hat{r}_{2,\bar{\mu}^m} \bar{\mu}^m + \hat{r}_{2,\bar{\zeta}^m} \cdot \bar{\zeta}^m. \quad (49h)$$

The sensitivities in (49) can be expressed in terms of the sensitivities with respect to μ , introduced in (48), cf. Appendix B.

6 Numerical study

6.1 Preliminaries

The single RVE depicted in Fig. 4, with randomly generated substructure, is used for all computations. The RVE is assumed to occupy the two-dimensional domain $\Omega_{\square}(\bar{\mathbf{x}}) = \{\mathbf{x} : \mathbf{x} - \bar{\mathbf{x}} \in (-0.5, 0.5) \times (-0.5, 0.5)\}$. Note that the matrix is contiguous, whereas the particles are completely embedded in the matrix. Thus, they can be close to each other, but never in direct contact. Note that there are no intersections of particles with the RVE boundary. This choice simplifies the mesh generation and is not a prerequisite of the applied method.

The numerical results are obtained using the Finite Element tool box Ferrite.jl [27] and visualized using the package Makie.jl [28]. Thereby, triangular elements with (the simplest possible) linear approximation are used.

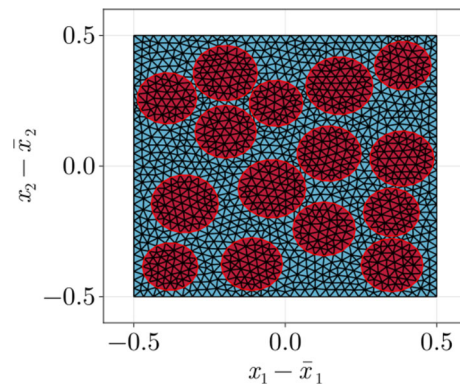


Fig. 4 Mesh for the RVE-problem. There is no overlap or direct contact of particles

The main goal of the conducted parametric study is to compare the performance of the dual potential approach with the single potential approach, representing standard first order homogenization. Firstly, the RVE responses for selected load cases are investigated. Secondly, the solutions for the different approaches are compared to DNS as reference. A simple example problem is considered, since the focus is solely on the performance in terms of the upscaled (macroscale) values. For this reason, all units are omitted. To simplify the problem, we choose the parameters

$$\mu_{\text{ref}} = 0, \quad c_{\text{ref}} = 0, \quad \frac{R\theta_{\text{ref}}}{c_m} = 1,$$

which imply the special case of $\mu = c$. Since different modes of the overall transport can be relevant, investigations for different values of the mobility ratio are of interest. To this end, the mobility η for the matrix is fixed, while the influence of different values of η for the particles and η_{if} at the interface is investigated. The considered parameter values are listed in Table 1.

6.2 RVE response

To demonstrate the behavior of the presented dual potential approaches, the RVE responses to selected load cases are investigated for low interface mobility (set 2 in Table 1). Specifically, the two unit load cases for $\bar{\zeta}^p = [1 \ 0]^T$ and $\bar{\zeta}^m = [1 \ 0]^T$ are considered in order to compute the relevant sensitivities.

The results for the gradient-based linear-linear description are depicted in Fig. 5. One can observe a problem due to the discontinuity of the particle phase: Inside each individual particle, the potential follows $\bar{\zeta}^p$ and is close to the potential in the surrounding matrix material, thereby minimizing the jump of μ across the interface. This representation of $\bar{\zeta}^p$ as “particle-wise gradient” can be observed in Fig. 5a. Since there is no overall change in potential across the RVE, this

Table 1 Investigated cases of material mobilities

Set	Label	η matrix	η particles	η_{if}
1	Nearly homogeneous	1	1	10^8
2	Low interface mobility	1	1	10^{-3}
3	Low interface mobility - conducting particles	1	10^5	10^{-3}
4	Very low interface mobility	1	1	10^{-5}

is not what we would consider as a physically representative macroscale gradient. Similarly, in Fig. 5b, there are changes in potential from particle to particle across the RVE, even though $\bar{\zeta}^P = \mathbf{0}$ is prescribed. In conclusion, $\bar{\zeta}^P$ is not represented correctly in the RVE response for the linear-linear prolongation with gradient-based constraints.

The issue above motivates the introduction of moment-based constraints for the linear-linear prolongation. To verify that this approach gives more accurate results, we consider the response to the same two unit load cases. This is depicted in Fig. 6. One can observe that $\bar{\zeta}^P$ is now reflected as a change in potential from particle to particle across the RVE, which is considered as a more accurate representation of the macroscale gradient.

6.3 Example problem

Next, an example problem is solved using the different approaches and the results are compared to a DNS. The mesh for the DNS problem is created based on 10 copies of the RVE mesh, which are arranged in a row and connected to each other. In the following, the parts of the DNS domain associated with the underlying RVE copies are referred to as DNS subdomains. The geometry and FE-mesh for the macroscale domain are shown in Fig. 7. The initial state is formally defined by the initial concentration c_0 , which (for a linear model) corresponds to the initial potential μ_0 . Here, we prescribe $\mu(t = 0) = \mu_0 = 0$, which corresponds to $c_0 = 0$ for the chosen parameters.

Furthermore, insulating ($j_n = 0$) boundary conditions are applied at the top, right and bottom side of the domain. On the left boundary, the potential is increased linearly from 0 to 1 over the time span $t \in (0, 10]$, whereafter it is held at 1. Clearly, for the DNS and the single potential approach these boundary conditions are applied to μ or $\bar{\mu}$, respectively. However, for the dual potential approach different choices are possible. Using the linear-linear prolongation, both $\bar{\mu}^m$ and $\bar{\mu}^P$ can be prescribed. For the constant-linear prolongation only $\bar{\mu}^m$ may be prescribed. To have consistent boundary conditions for all applied methods, we choose to apply the described ramp loading for $\bar{\mu}^m$ while complete insulation is chosen as the boundary condition associated with $\bar{\mu}^P$. This is also in good agreement with the DNS problem, where there is no flux from the boundary into the particle domain. In

general, appropriate boundary conditions may be derived by homogenizing a boundary layer.

The computation times of the presented multi-scale approaches relative to DNS are given in Table 2. The most important observations are:

- All multi-scale approaches require significantly less time than the DNS.
- Using dual potentials requires more time than using a single potential.
- The constant-linear prolongation requires less time than the linear-linear one.
- For the multi-scale approaches, computing the sensitivities takes more time than solving the macroscale problem.

Note that the considered example problem is relatively simple and the measured times are not representative for more complex problems. In such a case, it can be expected that the computation of the sensitivities will be less relevant for the overall computation time. Hence, the speed-up of the multi-scale models compared to DNS would be greater than the values in Table 2 indicate.

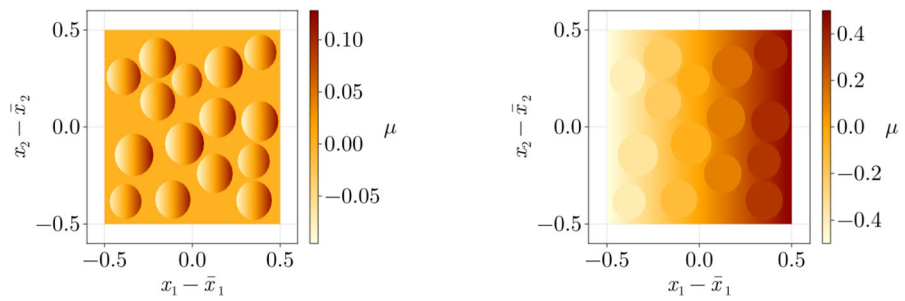
It remains to be analyzed how the methods perform regarding the quality of the solutions.

Selected snapshots of the DNS solution for low interface mobility (set 2 in Table 1) are depicted in Fig. 8 in order to demonstrate the system behavior over time. One can observe that the boundary conditions affect the potential inside the matrix and that the potential inside the particles adapts to the surrounding matrix potential with a certain time delay.

For the same set of material parameters, the results of the different methods at a fixed time $t = 50$ are collected in Fig. 10. To compare the DNS and the macroscale models, a fine-scale solution is reconstructed from the macroscale fields. This reconstruction is based on the DNS subdomains (cf. Figure 7a). Firstly, the macroscale fields are evaluated at the locations corresponding to the centers of the subdomains. Secondly, the solutions of the corresponding RVE-problems are computed and concatenated. An illustration of the reconstruction is given in Fig. 9.

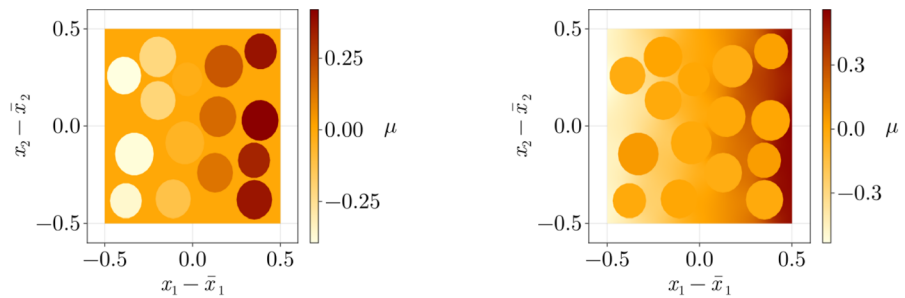
By a comparison of Fig. 10b with a, it becomes clear that the (conventional) single potential approach fails to describe the delayed increase in potential inside the particles. Moreover, the results from the constant-linear (Fig. 10c)

Fig. 5 RVE responses to two different load cases for the dual potential approach using a linear-linear prolongation with gradient-based constraints



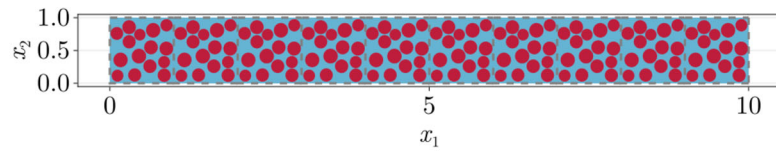
(a) $\bar{\mu}^P = 0, \bar{\zeta}^P = \begin{bmatrix} 1 \\ 0 \end{bmatrix}, \bar{\mu}^m = 0, \bar{\zeta}^m = \begin{bmatrix} 0 \\ 0 \end{bmatrix}.$ (b) $\bar{\mu}^P = 0, \bar{\zeta}^P = \begin{bmatrix} 0 \\ 0 \end{bmatrix}, \bar{\mu}^m = 0, \bar{\zeta}^m = \begin{bmatrix} 1 \\ 0 \end{bmatrix}.$

Fig. 6 RVE responses to two different load cases for the dual potential approach with the linear-linear prolongation and moment-based constraints

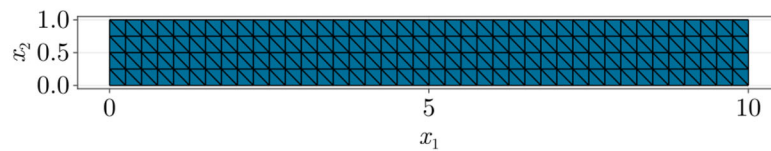


(a) $\bar{\mu}^P = 0, \bar{\zeta}^P = \begin{bmatrix} 1 \\ 0 \end{bmatrix}, \bar{\mu}^m = 0, \bar{\zeta}^m = \begin{bmatrix} 0 \\ 0 \end{bmatrix}.$ (b) $\bar{\mu}^P = 0, \bar{\zeta}^P = \begin{bmatrix} 0 \\ 0 \end{bmatrix}, \bar{\mu}^m = 0, \bar{\zeta}^m = \begin{bmatrix} 1 \\ 0 \end{bmatrix}.$

Fig. 7 Domains for the different problems in the numerical study



(a) Geometry for the DNS problem based on 10 copies of the RVE mesh. The DNS subdomains associated with the RVE copies are marked by gray, dashed boxes.



(b) Mesh for the macroscale problems.

Table 2 Computation times of solving the problem for low interface mobility (set 2 in Table 1) using different methods: t_{comp} denotes the computation time normalized with respect to the computation time of

the DNS, $t_{f,sens}$ denotes the fraction of the computation time needed to compute the sensitivities and $t_{f,solve}$ denotes the fraction needed to solve the macroscale problem

Method	t_{comp} [-]	$t_{f,sens}$ [%]	$t_{f,solve}$ [%]
DNS	1		
Single potential	0.0526	82.42	17.57
Dual potential, constant-linear, moment-based	0.0931	74.67	25.39
Dual potential, linear-linear, gradient-based	0.1344	82.95	17.05
Dual potential, linear-linear, moment-based	0.1444	83.72	16.28

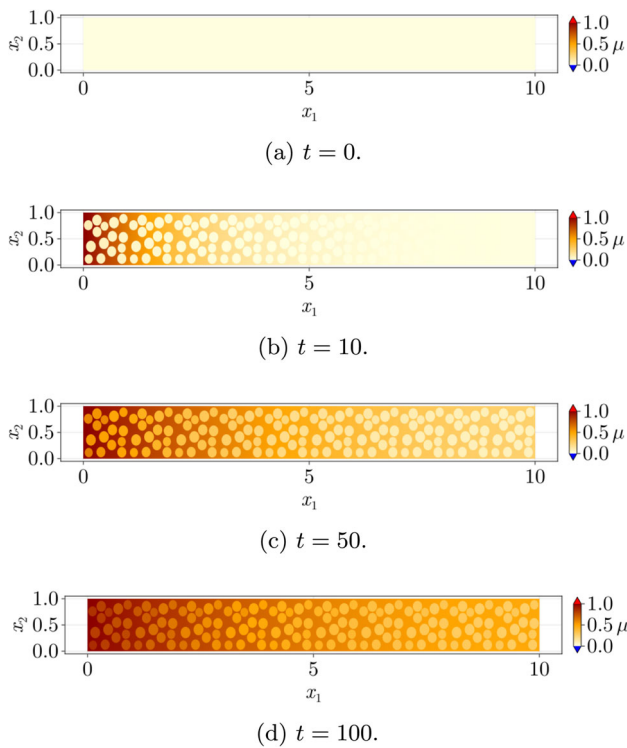
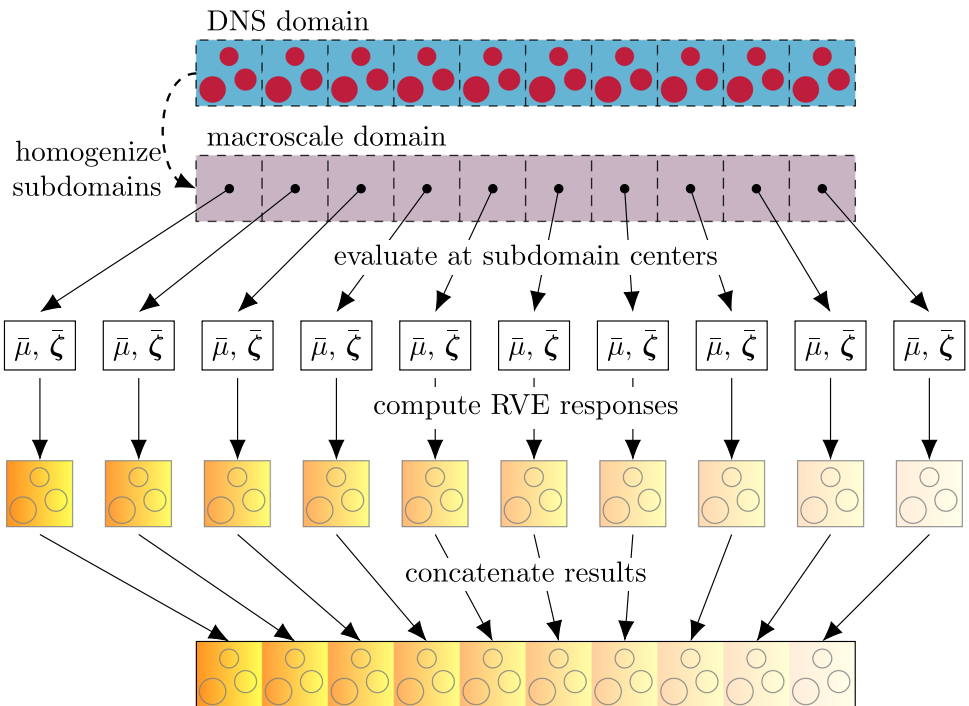


Fig. 8 DNS solution at different times for low interface mobility (set 2 in Table 1)

or linear-linear prolongation with moment-based constraints (Fig. 10e) appear to match the DNS very well. In contrast, the potential values for the linear-linear prolongation with

Fig. 9 Illustration of the reconstruction of a fine-scale solution from a macroscale solution for a single macroscale potential



gradient-based constraints (Fig. 10d) are visibly higher than for the DNS.

To compare the results in a more compact way, the concentration along the center line ($x_2 = 0.5$) through the domain for the macroscale problems (Fig. 7) is considered. The corresponding line plots are depicted in Fig. 11. To use the DNS as reference for the values obtained from the macroscale problems, we choose appropriate averages over the DNS subdomains. Compared to the DNS, a clear mismatch can be observed for the single potential approach and the dual potential approach using the linear-linear prolongation with gradient-based constraints (Fig. 11a). For constant-linear prolongation (Fig. 11b) and linear-linear prolongation with moment-based constraints (Fig. 11c), the results are significantly closer to the results from DNS.

Next, the time-dependent response is investigated and compared for different values of the mobilities. For this purpose, the total amount $C := \int_{\Omega} c \, d\Omega$ of the diffusing species inside the macroscale domain is considered. The computed results are collected in Fig. 12 for the different parameter values.

In case of a nearly homogeneous material (Fig. 12a), it can be observed that only the results for the constant-linear prolongation deviate significantly from the DNS. This is a result of the neglected part of the potential gradient.

For the cases with low (Fig. 12b and d) or very low (Fig. 12c) interface mobility, the constant-linear prolongation gives the more accurate results. Note that the constant-linear prolongation is motivated by the assumption that the transport through the microstructure is not significantly affected

Fig. 10 Solutions at $t = 50$ for low interface mobility (set 2 in Table 1). For the macroscale models, a sub-scale solution is reconstructed based on the DNS subdomains (cf. Figure 7a). For each subdomain, the solution of an RVE-problem is computed and used as representation of the fine-scale solution within the subdomain. As a result, potential jumps between the DNS subdomains are possible, although they are hardly visible. In addition to the solution field, the relative error $e_\mu := \frac{|\mu - \mu_{\text{DNS}}|}{\max(|\mu_{\text{DNS}}|)}$ with the DNS solution μ_{DNS} as reference is depicted

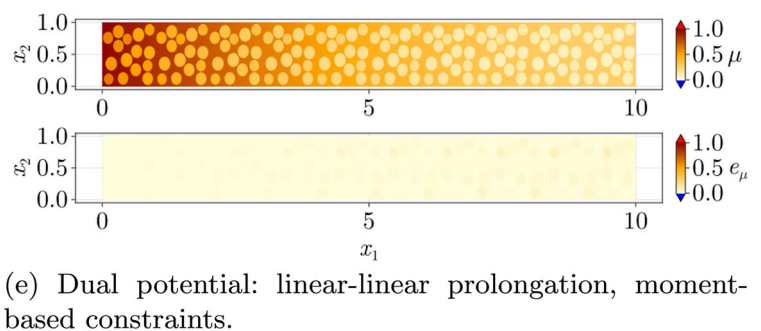
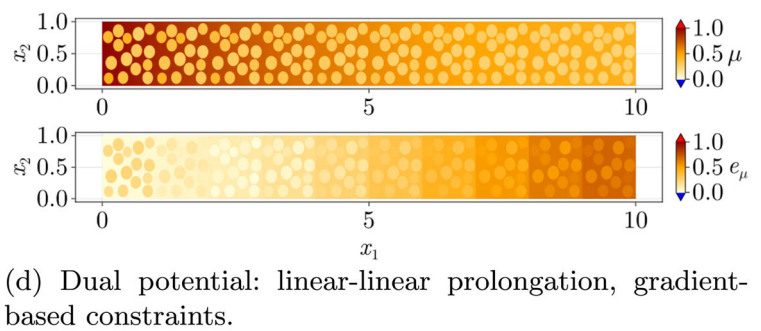
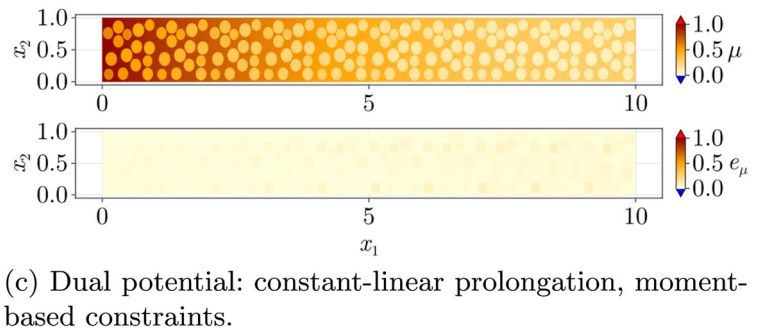
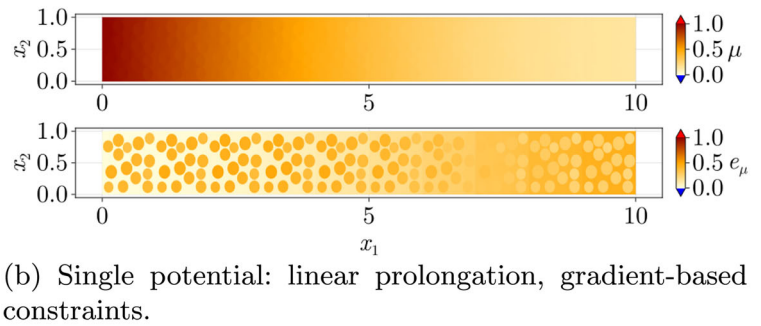
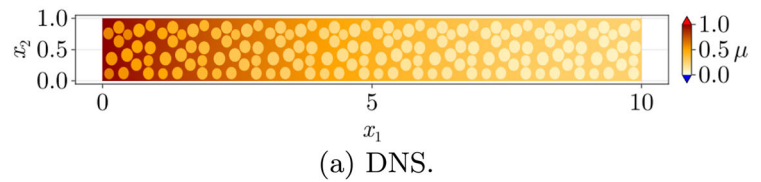


Fig. 11 Concentration at $t = 50$ along the center line of the domain for low interface mobility (set 2 in Table 1). Each subfigure shows a comparison of results from one specific algorithmic version of the dual potential approach with results from DNS and the single potential approach (with gradient-based constraints). For the DNS, macroscale values are obtained by averaging over the DNS subdomains

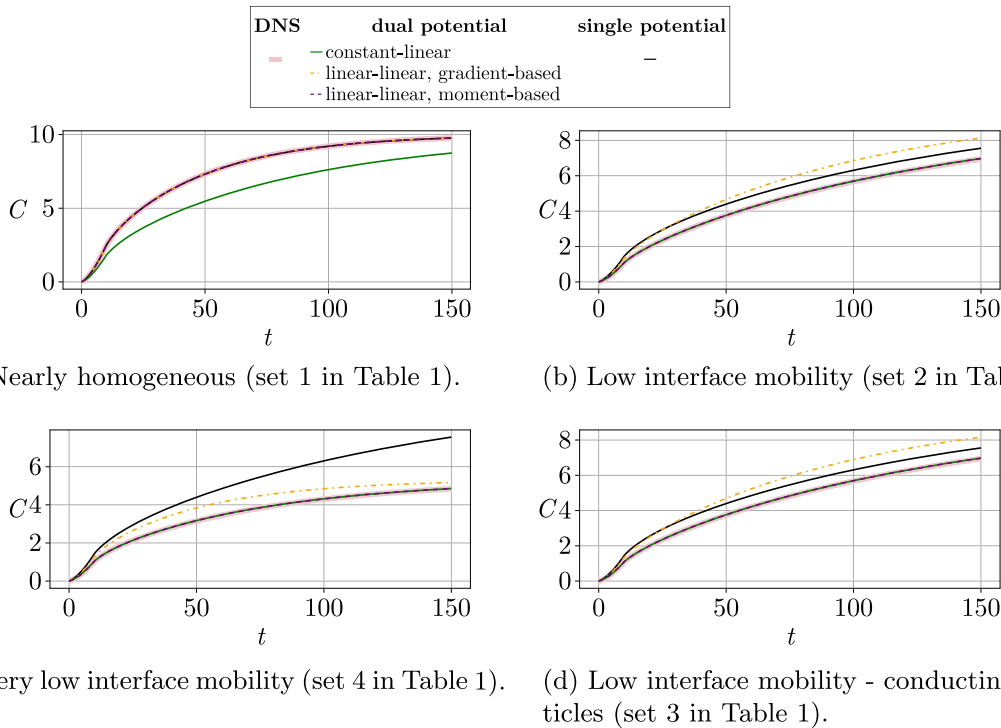
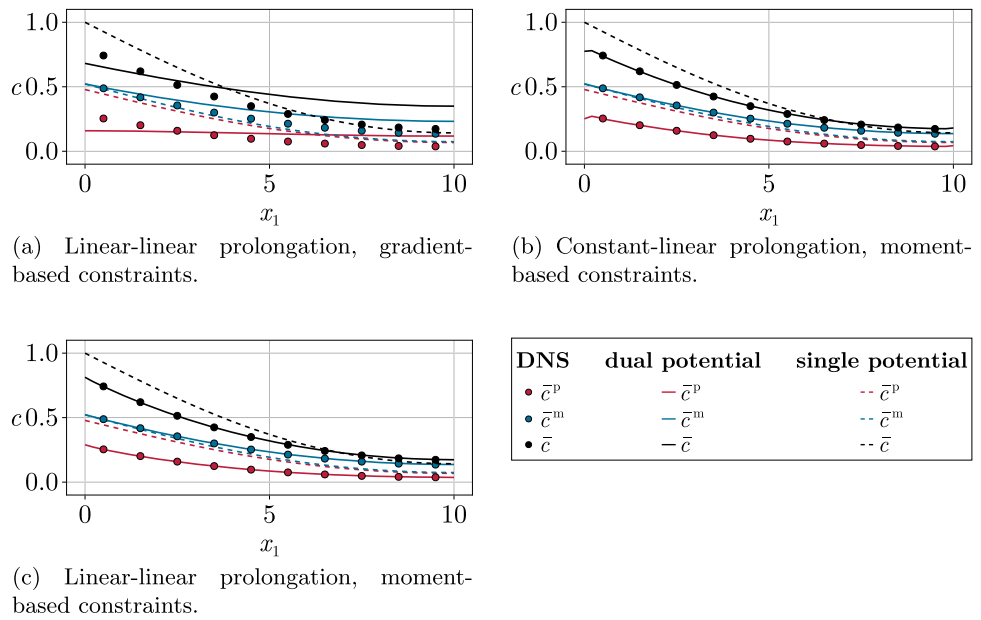


Fig. 12 Development with time of the total amount (in moles) of the diffusing species in the entire macroscale domain. Each diagram shows results for the different material parameter values listed in Table 1

by flux through individual particles. Since a difference in particle mobility does not affect the results visibly (compare Fig. 12b to d), this assumption appears to be appropriate in these cases.

In contrast to the constant-linear prolongation, the single potential approach and the linear-linear prolongation with gradient-based constraints lead to a larger mismatch with the DNS when the interface mobility is low. Obviously, the single

potential approach can not accurately capture the transient effects due to the resistance at the interface. For linear-linear prolongation with gradient-based based constraints, the effective mobility is not estimated accurately due to the particle-wise gradients in the RVE response (cf. Figure 5), which explains the mismatch with the DNS (cf. Figure 12b, c and d).

It is only for linear-linear prolongation with moment-based constraints that the results match the DNS well for all investigated mobility values. However, when the interface resistance is sufficiently high, then the results for the constant-linear prolongation are equally accurate. In this case, choosing the constant-linear prolongation appears to be advantageous, since the macroscale model becomes significantly less complex (despite a system of dual potentials).

7 Conclusion and outlook

Efficient procedures for computational homogenization, based on the VCH concept, of linear transient diffusion transport in particle-matrix composites with material interfaces are investigated. Focus is placed on their ability to accurately represent the macroscale (homogenized) response under the assumption of micro-stationarity, which allows for direct upscaling.

Firstly, from the numerical results it is concluded that the performance of the classical approach, based on a single macroscale potential, is not satisfactory in the present setup based on micro-stationarity. The insufficiency is obviated by the fact that the transport across the interface between particle and matrix does not appear in the macroscale problem. This is particularly pronounced when the interface resistance is large.

As a remedy, the non-classical approach of dual potentials (one for each phase) is then introduced. Different assumptions are introduced with respect to (i) prolongation order and (ii) homogenization constraints, giving rise to different algorithms. These algorithms are assessed in light of DNS applied to a two-dimensional test problem. Based on this limited numerical evaluation, we conclude that one of the investigated algorithms gives accurate results for the entire range of material parameter values (that are considered in this paper): The linear-linear prolongation with moment-based homogenization constraints. For the constant-linear prolongation, the performance depends on the actual values of material parameters; however, this method implies a less complex macroscale model with reduced computational cost as a consequence.

A general conclusion for the dual potential approach (for both the linear-linear and the constant-linear prolongation) is that the accuracy is increased when (the classical) gradient-based homogenization constraint is replaced by the moment-based one.

Future investigations should include a direct comparison with RVE-formulations as part of full-fledged transient homogenization. Further, nonlinearities in the constitutive models are inevitable to accurately describe real world problems. Finally, it is of significant engineering interest

to consider coupled transport problems such as electrochemical interactions in battery electrode materials. Clearly, the goal is to devise reliable criteria, based on a posteriori error control, for the choice of the most efficient algorithm given the properties of the underlying fine-scale problem (multiphysics couplings, material parameters, interface characteristics, nonlinear effects, etc).

Appendix A Variationally consistent macro-homogeneity condition

To elaborate on the macro-homogeneity condition (or generalized Hill-Mandel condition) for the dual potential approach, we discuss the case of constant-linear prolongation with moment-based constraints. For given macroscale perturbations $d\bar{\mu}^p(t)$, $d\bar{\mu}^m(t)$ and $d\bar{\xi}^m(t)$ pertinent to the macroscopic formulation in (28), we observe the resulting sub-scale sensitivity $d\mu(t)$ from (35). Next, we choose the test function $\delta\mu = d\mu - \mu^M[d\bar{\mu}^p, d\bar{\mu}^m, d\bar{\xi}^m]$ for the presented RVE-problem (35). The balance equation (35a) can then be rewritten as

$$\begin{aligned} & \langle \partial_t c d\mu \rangle_{\square} - \langle \mathbf{j} \cdot d\boldsymbol{\xi} \rangle_{\square} - \langle \langle \mathbf{j}_n \llbracket d\mu \rrbracket \rangle \rangle_{\square}^i \\ & + \bar{\lambda}_{\mu}^p \langle d\mu \rangle^p + \bar{\lambda}_{\mu}^m \langle d\mu \rangle^m + \bar{\lambda}_{\xi}^m \cdot \langle d\mu [\mathbf{x} - \bar{\mathbf{x}}] \rangle^m \\ & + \frac{1}{|\Omega_{\square}|} \int_{\Gamma_{\square}^{\pm}} \lambda \llbracket d\mu \rrbracket_{\square} d\Gamma \\ & = \partial_t \bar{c}^p d\bar{\mu}^p + \partial_t \bar{c}^m d\bar{\mu}^m - \left[\bar{\mathbf{j}}^m - \partial_t \bar{\mathbf{c}}_2^m + \bar{\mathbf{r}}_2 \right] \cdot d\bar{\xi}^m \\ & - \bar{r} \left[d\bar{\mu}^m - d\bar{\mu}^p \right] \\ & + \bar{\lambda}_{\mu}^p d\bar{\mu}^p + \bar{\lambda}_{\mu}^m \left[d\bar{\mu}^m + d\bar{\xi}^m \cdot \left[\langle \mathbf{x} \rangle^m - \bar{\mathbf{x}} \right] \right] + \bar{\lambda}_{\xi}^m \\ & \cdot \left[d\bar{\xi}^m \cdot \left[\langle \mathbf{x} - \bar{\mathbf{x}} \rangle \otimes [\mathbf{x} - \bar{\mathbf{x}}] \right]^m + \left[d\bar{\mu}^m \left[\langle \mathbf{x} \rangle^m - \bar{\mathbf{x}} \right] \right] \right] \\ & + \frac{1}{|\Omega_{\square}|} \int_{\Gamma_{\square}^{m+}} \lambda \llbracket \mathbf{x} \rrbracket_{\square} d\Gamma \cdot d\bar{\xi}^m, \end{aligned} \quad (\text{A1})$$

using the notation $d\boldsymbol{\xi} := \nabla d\mu$.

To obtain the macro-homogeneity condition, the terms for the Lagrange multipliers need to be eliminated. We can exploit the linearity of the constraints (35b) to (35e) by choosing $\delta\bar{\lambda}_{\mu}^p = \bar{\lambda}_{\mu}^p$, $\delta\bar{\lambda}_{\mu}^m = \bar{\lambda}_{\mu}^m$, $\delta\bar{\lambda}_{\xi}^m = \bar{\lambda}_{\xi}^m$ and $\delta\lambda = \lambda$ to obtain the identities

$$\bar{\lambda}_{\mu}^p \langle d\mu \rangle^p = \bar{\lambda}_{\mu}^p d\bar{\mu}^p, \quad (\text{A2a})$$

$$\bar{\lambda}_{\mu}^m \langle d\mu \rangle^m = \bar{\lambda}_{\mu}^m \left[d\bar{\mu}^m + d\bar{\xi}^m \cdot \left[\langle \mathbf{x} \rangle^m - \bar{\mathbf{x}} \right] \right], \quad (\text{A2b})$$

$$\begin{aligned} \bar{\lambda}_{\xi}^m \cdot \langle d\mu [\mathbf{x} - \bar{\mathbf{x}}] \rangle^m & = \bar{\lambda}_{\xi}^m \cdot \left[d\bar{\xi}^m \cdot \left[\langle \mathbf{x} - \bar{\mathbf{x}} \rangle \otimes [\mathbf{x} - \bar{\mathbf{x}}] \right]^m \right. \\ & \left. + \left[d\bar{\mu}^m \left[\langle \mathbf{x} \rangle^m - \bar{\mathbf{x}} \right] \right] \right], \end{aligned} \quad (\text{A2c})$$

$$\frac{1}{|\Omega_\square|} \int_{\Gamma_\square^+} \lambda \llbracket d\mu \rrbracket_\square d\Gamma = \frac{1}{|\Omega_\square|} \int_{\Gamma_\square^{m+}} \lambda \llbracket \mathbf{x} \rrbracket_\square d\Gamma \cdot d\bar{\xi}^m. \tag{A2d}$$

Insertion of (A2) into (A1) results in

$$\begin{aligned} & \langle \partial_t c d\mu \rangle_\square - \langle \mathbf{j} \cdot d\boldsymbol{\xi} \rangle_\square - \langle \langle j_n \llbracket d\mu \rrbracket \rangle \rangle_\square^i \\ &= \partial_t \bar{c}^p d\bar{\mu}^p + \partial_t \bar{c}^m d\bar{\mu}^m - \left[\bar{\mathbf{j}}^m - \partial_t \bar{c}_2^m + \bar{\mathbf{r}}_2 \right] \cdot d\bar{\xi}^m \\ & \quad - \bar{r} \left[d\bar{\mu}^m - d\bar{\mu}^p \right], \end{aligned} \tag{A3}$$

which can be identified as the macro-homogeneity condition. This condition is contained in the presented RVE-problem.

Note that one would obtain the same result for gradient-based constraints, because the corresponding terms of the constraints can be eliminated in the same manner. Analogously, one can derive the macro-homogeneity condition for the linear-linear prolongation, cf. (47), which reads

$$\begin{aligned} & \langle \partial_t c d\mu \rangle_\square - \langle \mathbf{j} \cdot d\boldsymbol{\xi} \rangle_\square - \langle \langle j_n \llbracket d\mu \rrbracket \rangle \rangle_\square^i \\ &= \partial_t \bar{c}^p d\bar{\mu}^p + \partial_t \bar{c}^m d\bar{\mu}^m - \left[\bar{\mathbf{j}}^p - \partial_t \bar{c}_2^p - \bar{\mathbf{r}}_2 \right] \cdot d\bar{\xi}^p \\ & \quad - \left[\bar{\mathbf{j}}^m - \partial_t \bar{c}_2^m + \bar{\mathbf{r}}_2 \right] \cdot d\bar{\xi}^m - \bar{r} \left[d\bar{\mu}^m - d\bar{\mu}^p \right]. \end{aligned} \tag{A4}$$

A more specific form of (A3) follows by repeating the steps above for the solution itself, i.e. considering $\bar{\mu}^p, \bar{\mu}^m, \bar{\xi}^m \rightarrow \mu$, rather than the arbitrary perturbation. We then obtain

$$\begin{aligned} & \langle \partial_t c \mu \rangle_\square - \langle \mathbf{j} \cdot \boldsymbol{\xi} \rangle_\square - \langle \langle j_n \llbracket \mu \rrbracket \rangle \rangle_\square^i \\ &= \partial_t \bar{c}^p \bar{\mu}^p + \partial_t \bar{c}^m \bar{\mu}^m - \left[\bar{\mathbf{j}}^m - \partial_t \bar{c}_2^m + \bar{\mathbf{r}}_2 \right] \cdot \bar{\xi}^m - \bar{r} \left[\bar{\mu}^m - \bar{\mu}^p \right]. \end{aligned} \tag{A5}$$

To further elaborate the properties of the VCH approach, we consider the thermodynamic properties as follows. The isothermal transport problem can be formulated in terms of a free energy $\psi(c)$ such that $\mu = \frac{\partial \psi}{\partial c}$ and the dissipation terms due to transport become

$$D_\Omega = -\mathbf{j} \cdot \boldsymbol{\xi} \quad \text{in } \Omega_\square^p \cup \Omega_\square^m, \tag{A6a}$$

$$D_\Gamma = -j_n \llbracket \mu \rrbracket \quad \text{on } \Gamma^i, \tag{A6b}$$

respectively. From (A5), we thus conclude that

$$\begin{aligned} & \langle \partial_t \psi \rangle_\square + \langle D_\Omega \rangle_\square + \langle \langle D_\Gamma \rangle \rangle_\square^i = \partial_t \bar{c}^p \bar{\mu}^p + \partial_t \bar{c}^m \bar{\mu}^m \\ & \quad - \left[\bar{\mathbf{j}}^m - \partial_t \bar{c}_2^m + \bar{\mathbf{r}}_2 \right] \cdot \bar{\xi}^m - \bar{r} \left[\bar{\mu}^m - \bar{\mu}^p \right]. \end{aligned} \tag{A7}$$

Hence, the sum of the rate of the free energy and the dissipation is consistently upscaled.

Appendix B Sensitivities

$$\bar{c}_l^p = \langle c(\mu_l) \rangle_\square^p, \quad \bar{c}_l^m = \langle c(\mu_l) \rangle_\square^m, \tag{B8a}$$

$$\hat{\bar{c}}_{\bar{\mu}^p}^p = \langle c(\hat{\mu}_{\bar{\mu}^p}) \rangle_\square^p, \quad \hat{\bar{c}}_{\bar{\mu}^p}^m = \langle c(\hat{\mu}_{\bar{\mu}^p}) \rangle_\square^m, \tag{B8b}$$

$$(\hat{\bar{c}}_{\bar{\xi}^p}^p)_i = \langle c((\hat{\mu}_{\bar{\xi}^p})_i) \rangle_\square^p, \quad (\hat{\bar{c}}_{\bar{\xi}^p}^m)_i = \langle c((\hat{\mu}_{\bar{\xi}^p})_i) \rangle_\square^m, \tag{B8c}$$

$$\hat{\bar{c}}_{\bar{\mu}^m}^p = \langle c(\hat{\mu}_{\bar{\mu}^m}) \rangle_\square^p, \quad \hat{\bar{c}}_{\bar{\mu}^m}^m = \langle c(\hat{\mu}_{\bar{\mu}^m}) \rangle_\square^m, \tag{B8d}$$

$$(\hat{\bar{c}}_{\bar{\xi}^m}^p)_i = \langle c((\hat{\mu}_{\bar{\xi}^m})_i) \rangle_\square^p, \quad (\hat{\bar{c}}_{\bar{\xi}^m}^m)_i = \langle c((\hat{\mu}_{\bar{\xi}^m})_i) \rangle_\square^m, \tag{B8e}$$

$$\bar{c}_{2,l}^p = \langle c(\mu_l) [\mathbf{x} - \bar{\mathbf{x}}] \rangle_\square^p,$$

$$\bar{c}_{2,l}^m = \langle c(\mu_l) [\mathbf{x} - \bar{\mathbf{x}}] \rangle_\square^m, \tag{B9a}$$

$$\hat{\bar{c}}_{2,\bar{\mu}^p}^p = \langle c(\hat{\mu}_{\bar{\mu}^p}) [\mathbf{x} - \bar{\mathbf{x}}] \rangle_\square^p,$$

$$\hat{\bar{c}}_{2,\bar{\mu}^p}^m = \langle c(\hat{\mu}_{\bar{\mu}^p}) [\mathbf{x} - \bar{\mathbf{x}}] \rangle_\square^m, \tag{B9b}$$

$$(\hat{\bar{c}}_{2,\bar{\xi}^p}^p)_{ij} = \langle (\mathbf{x} - \bar{\mathbf{x}})_i c((\hat{\mu}_{\bar{\xi}^p})_j) \rangle_\square^p,$$

$$(\hat{\bar{c}}_{2,\bar{\xi}^p}^m)_{ij} = \langle (\mathbf{x} - \bar{\mathbf{x}})_i c((\hat{\mu}_{\bar{\xi}^p})_j) \rangle_\square^m, \tag{B9c}$$

$$\hat{\bar{c}}_{2,\bar{\mu}^m}^p = \langle c(\hat{\mu}_{\bar{\mu}^m}) [\mathbf{x} - \bar{\mathbf{x}}] \rangle_\square^p,$$

$$\hat{\bar{c}}_{2,\bar{\mu}^m}^m = \langle c(\hat{\mu}_{\bar{\mu}^m}) [\mathbf{x} - \bar{\mathbf{x}}] \rangle_\square^m, \tag{B9d}$$

$$(\hat{\bar{c}}_{2,\bar{\xi}^m}^p)_{ij} = \langle (\mathbf{x} - \bar{\mathbf{x}})_i c((\hat{\mu}_{\bar{\xi}^m})_j) \rangle_\square^p,$$

$$(\hat{\bar{c}}_{2,\bar{\xi}^m}^m)_{ij} = \langle (\mathbf{x} - \bar{\mathbf{x}})_i c((\hat{\mu}_{\bar{\xi}^m})_j) \rangle_\square^m, \tag{B9e}$$

$$\bar{\mathbf{j}}_l^p = \langle -\mathbf{M} \cdot \boldsymbol{\xi} [\mu_l] \rangle_\square^p,$$

$$\bar{\mathbf{j}}_l^m = \langle -\mathbf{M} \cdot \boldsymbol{\xi} [\mu_l] \rangle_\square^m, \tag{B10a}$$

$$\hat{\bar{\mathbf{j}}}_{\bar{\mu}^p}^p = \langle -\mathbf{M} \cdot \boldsymbol{\xi} [\hat{\mu}_{\bar{\mu}^p}] \rangle_\square^p,$$

$$\hat{\bar{\mathbf{j}}}_{\bar{\mu}^p}^m = \langle -\mathbf{M} \cdot \boldsymbol{\xi} [\hat{\mu}_{\bar{\mu}^p}] \rangle_\square^m, \tag{B10b}$$

$$\hat{\bar{\mathbf{j}}}_{\bar{\xi}^p}^p = \sum_i \langle -\mathbf{M} \cdot \boldsymbol{\xi} [(\hat{\mu}_{\bar{\xi}^p})_i] \rangle_\square^p \otimes \mathbf{e}_i,$$

$$\hat{\bar{\mathbf{j}}}_{\bar{\xi}^p}^m = \sum_i \langle -\mathbf{M} \cdot \boldsymbol{\xi} [(\hat{\mu}_{\bar{\xi}^p})_i] \rangle_\square^m \otimes \mathbf{e}_i \tag{B10c}$$

$$\hat{\bar{\mathbf{j}}}_{\bar{\mu}^m}^p = \langle -\mathbf{M} \cdot \boldsymbol{\xi} [\hat{\mu}_{\bar{\mu}^m}] \rangle_\square^p,$$

$$\hat{\bar{\mathbf{j}}}_{\bar{\mu}^m}^m = \langle -\mathbf{M} \cdot \boldsymbol{\xi} [\hat{\mu}_{\bar{\mu}^m}] \rangle_\square^m, \tag{B10d}$$

$$\hat{\bar{\mathbf{j}}}_{\bar{\xi}^m}^p = \sum_i \langle -\mathbf{M} \cdot \boldsymbol{\xi} [(\hat{\mu}_{\bar{\xi}^m})_i] \rangle_\square^p \otimes \mathbf{e}_i,$$

$$\hat{\bar{\mathbf{j}}}_{\bar{\xi}^m}^m = \sum_i \langle -\mathbf{M} \cdot \boldsymbol{\xi} [(\hat{\mu}_{\bar{\xi}^m})_i] \rangle_\square^m \otimes \mathbf{e}_i, \tag{B10e}$$

$$\bar{r}_l = \langle \langle -\eta_{if} \llbracket \mu_l \rrbracket \rangle \rangle_\square^i, \quad \bar{r}_{2,l} = \langle \langle -\eta_{if} \llbracket \mu_l \rrbracket [\mathbf{x} - \bar{\mathbf{x}}] \rangle \rangle_\square^i,$$

$$\hat{\bar{r}}_{\bar{\mu}^p} = \langle \langle -\eta_{if} \llbracket \hat{\mu}_{\bar{\mu}^p} \rrbracket \rangle \rangle_\square^i, \quad \hat{\bar{r}}_{2,\bar{\mu}^p} = \langle \langle -\eta_{if} \llbracket \hat{\mu}_{\bar{\mu}^p} \rrbracket [\mathbf{x} - \bar{\mathbf{x}}] \rangle \rangle_\square^i, \tag{B11a}$$

$$(\hat{\bar{r}}_{2,\bar{\xi}^p})_{ij} = \langle \langle -\eta_{if} \llbracket (\hat{\mu}_{\bar{\xi}^p})_j \rrbracket [\mathbf{x} - \bar{\mathbf{x}}] \rangle \rangle_\square^i,$$

$$\hat{\bar{r}}_{2,\bar{\mu}^m} = \langle \langle -\eta_{if} \llbracket \hat{\mu}_{\bar{\mu}^m} \rrbracket [\mathbf{x} - \bar{\mathbf{x}}] \rangle \rangle_\square^i, \tag{B11b}$$

$$(\hat{\bar{r}}_{2,\bar{\xi}^m})_{ij} = \langle \langle -\eta_{if} \llbracket (\hat{\mu}_{\bar{\xi}^m})_j \rrbracket [\mathbf{x} - \bar{\mathbf{x}}] \rangle \rangle_\square^i. \tag{B11c}$$

$$\hat{\bar{r}}_{2,\bar{\mu}^m} = \langle \langle -\eta_{if} \llbracket \hat{\mu}_{\bar{\mu}^m} \rrbracket [\mathbf{x} - \bar{\mathbf{x}}] \rangle \rangle_\square^i, \tag{B11d}$$

$$(\hat{\bar{r}}_{2,\bar{\xi}^m})_{ij} = \langle \langle -\eta_{if} \llbracket (\hat{\mu}_{\bar{\xi}^m})_j \rrbracket [\mathbf{x} - \bar{\mathbf{x}}] \rangle \rangle_\square^i. \tag{B11e}$$

Acknowledgements This research was funded by the Swedish Research Council (VR) via grant Nos. 2020-05057 and 2019-05080, and by the Deutsche Forschungsgemeinschaft (DFG, German Research Foundation, GRK 2075), which is gratefully acknowledged.

Funding Open Access funding enabled and organized by Projekt DEAL.

Open Access This article is licensed under a Creative Commons Attribution 4.0 International License, which permits use, sharing, adaptation, distribution and reproduction in any medium or format, as long as you give appropriate credit to the original author(s) and the source, provide a link to the Creative Commons licence, and indicate if changes were made. The images or other third party material in this article are included in the article's Creative Commons licence, unless indicated otherwise in a credit line to the material. If material is not included in the article's Creative Commons licence and your intended use is not permitted by statutory regulation or exceeds the permitted use, you will need to obtain permission directly from the copyright holder. To view a copy of this licence, visit <http://creativecommons.org/licenses/by/4.0/>.

References

- Steinmann P, Häsner O (2005) On material interfaces in thermo-mechanical solids. *Arch Appl Mech* 75:31–41. <https://doi.org/10.1007/s00419-005-0383-8>
- Kaiser T, Menzel A (2021) Fundamentals of electro-mechanically coupled cohesive zone formulations for electrical conductors. *Comput Mech* 68:51–67. <https://doi.org/10.1007/s00466-021-02019-z>
- Javili A, Kaessmair S, Steinmann P (2014) General imperfect interfaces. *Comput Methods Appl Mech Eng* 275:76–97. <https://doi.org/10.1016/j.cma.2014.02.022>
- Javili A, Steinmann P, Mosler J (2017) Micro-to-macro transition accounting for general imperfect interfaces. *Comput Methods Appl Mech Eng* 317:274–317. <https://doi.org/10.1016/j.cma.2016.12.025>
- Firooz S, Steinmann P, Javili A (2021) Homogenization of composites with extended general interfaces: comprehensive review and unified modeling. *Appl Mech Rev* 73(4):040802. <https://doi.org/10.1115/1.4051481>
- Geers MGD, Kouznetsova VG, Brekelmans WAM (2010) Multi-scale computational homogenization: trends and challenges. *J Comput Appl Math* 234(7):2175–2182. <https://doi.org/10.1016/j.cam.2009.08.077>
- Saeb S, Steinmann P, Javili A (2016) Aspects of computational homogenization at finite deformations: a unifying review from Reuss' to Voigt's bound. *Appl Mech Rev* 68(5):050801. <https://doi.org/10.1115/1.4034024>
- Matouš K, Geers MGD, Kouznetsova VG, Gillman A (2017) A review of predictive nonlinear theories for multiscale modeling of heterogeneous materials. *J Comput Phys* 330:192–220. <https://doi.org/10.1016/j.jcp.2016.10.070>
- Salvadori A, Bosco E, Grazioli D (2014) A computational homogenization approach for Li-ion battery cells: Part I - formulation. *J Mech Phys Solids* 65:114–137. <https://doi.org/10.1016/j.jmps.2013.08.010>
- Güzel D, Kaiser T, Menzel A (2023) A computational multiscale approach towards the modelling of microstructures with material interfaces in electrical conductors. *Math Mech Solids*. <https://doi.org/10.1177/10812865231202721>
- Kaiser T, von der Höh N, Menzel A (2024) Computational multiscale modelling of material interfaces in electrical conductors. *J Mech Phys Solids* 186:105601. <https://doi.org/10.1016/j.jmps.2024.105601>
- Wu T, Temizer I, Wriggers P (2013) Computational thermal homogenization of concrete. *Cem Concr Compos* 35(1):59–70. <https://doi.org/10.1016/j.cemconcomp.2012.08.026>
- Wang M, Bu S, Zhou B, Li Z, Chen D (2023) Multi-scale heat conduction models with improved equivalent thermal conductivity of TRISO fuel particles for FCM fuel. *Nucl Eng Technol* 55(3):1140–1151. <https://doi.org/10.1016/j.net.2022.12.001>
- Özdemir I, Brekelmans WAM, Geers MGD (2008) Computational homogenization for heat conduction in heterogeneous solids. *Int J Numer Methods Eng* 73(2):185–204. <https://doi.org/10.1002/nme.2068>
- Zhuo M (2021) FE² multi-scale framework for the two-equation model of transient heat conduction in two-phase media. *Int J Heat Mass Transf* 179:121683. <https://doi.org/10.1016/j.ijheatmasstransfer.2021.121683>
- Larsson F, Runesson K, Su F (2010) Variationally consistent computational homogenization of transient heat flow. *Int J Numer Methods Eng* 81(13):1659–1686. <https://doi.org/10.1002/nme.2747>
- Brassart L, Stainier L (2019) Effective transient behaviour of heterogeneous media in diffusion problems with a large contrast in the phase diffusivities. *J Mech Phys Solids* 124:366–391. <https://doi.org/10.1016/j.jmps.2018.10.021>
- Brassart L, Stainier L (2018) Effective transient behaviour of inclusions in diffusion problems. *J Appl Math Mech* 98(6):981–998. <https://doi.org/10.1002/zamm.201700187>
- Waseem A, Heuzé T, Stainier L, Geers MGD, Kouznetsova VG (2021) Two-scale analysis of transient diffusion problems through a homogenized enriched continuum. *Eur J Mech A Solids* 87:104212. <https://doi.org/10.1016/j.euromechsol.2021.104212>
- Kaessmair S, Runesson K, Steinmann P, Jänicke R, Larsson F (2021) Variationally consistent computational homogenization of chemomechanical problems with stabilized weakly periodic boundary conditions. *Int J Numer Meth Eng* 122(22):6429–6454. <https://doi.org/10.1002/nme.6798>
- Rollin DR, Larsson F, Runesson K, Jänicke R (2023) Upscaling of chemo-mechanical properties of battery electrode material. *Int J Solids Struct* 281:112405. <https://doi.org/10.1016/j.ijsolstr.2023.112405>
- Sandström C, Larsson F (2013) Variationally consistent homogenization of Stokes flow in porous media. *Int J Multiscale Comput Eng* 11(2):117–138. <https://doi.org/10.1615/IntJMultCompEng.2012004069>
- Tu V, Larsson F, Runesson K, Jänicke R (2023) Variationally consistent homogenization of electrochemical ion transport in a porous structural battery electrolyte. *Eur J Mech A Solids* 98:104901. <https://doi.org/10.1016/j.euromechsol.2022.104901>
- Gandomkar A, Gray KE (2018) Local thermal non-equilibrium in porous media with heat conduction. *Int J Heat Mass Transf* 124:1212–1216. <https://doi.org/10.1016/j.ijheatmasstransfer.2018.04.011>
- Auriault, J-L., Boutin, C and Geindreau, C (2009) Heat transfer in composite materials. In: Auriault JL, Boutin C, Geindreau C (eds) *Homogenization of coupled phenomena in heterogeneous media*. Wiley, pp 107–142. <https://doi.org/10.1002/9780470612033.ch4>
- Kaessmair S, Steinmann P (2016) Comparative computational analysis of the Cahn-Hilliard equation with emphasis on C¹-continuous methods. *J Comput Phys* 322:783–803. <https://doi.org/10.1016/j.jcp.2016.07.005>
- Carlsson K, Ekre F, Ferrite.jl contributors. *Ferrite.jl*. <https://github.com/Ferrite-FEM/Ferrite.jl>
- Danisch S, Krumbiegel J (2021) Makie.jl: flexible high-performance data visualization for Julia. *J Open Source Softw* 6(65):3349. <https://doi.org/10.21105/joss.03349>

Publisher's Note Springer Nature remains neutral with regard to jurisdictional claims in published maps and institutional affiliations.